

1 **Reply to Referee #1**

2  
3 Ref: Atmos. Chem. Phys. Discuss., <https://doi.org/10.5194/acp-2018-1361-RC1>, Apr 04, 2019  
4 Title: “Winter 2018 major sudden stratospheric warming impact on midlatitude mesosphere from microwave  
5 radiometer measurements” by Yuke Wang et al.  
6

7 Dear Referee #1

8  
9 We thank Referee #1 for useful comments, discussion and proposals for corrections. We made corrections and  
10 changed the text according to the suggestions. Our revisions and reply to Referee #1 comment are below in blue  
11 colored text.

12  
13 **Referee Comment: RC**

14 **Authors Comment: AC**

15  
16 RC: GENERAL COMMENTS

17  
18 The topic of ground-based mesospheric carbon dioxide observations is interesting and fits into the scope of  
19 ACP. The local microwave radiometer observations over Kharkiv during the major warming event in 2018 are  
20 valuable, but they need to be validated and explained adequately. In this sense I suggest the authors to add  
21 stratospheric carbon dioxide and mesospheric temperature data for a solid discussion of horizontal and vertical  
22 transports. If this information is provided in a concentrated form during a \*major revision\*, the paper would  
23 gain further value.

24  
25 **AC: CO and mesospheric temperature data horizontal and vertical transports are included in new Sect.**  
26 **4.1 and 4.3: 4.1 CO variability 4.3 Temperature changes.**

27  
28 RC: SPECIFIC COMMENTS

29  
30 RC: 1) Validation: A validation of the reported CO observations is required. For this purpose satellite  
31 observations could be used 1) to compare the CO in the 60-90 km range and 2) to extend the profiles will into  
32 the stratosphere. This would allow the qualification of **downward transport** during the 2018 major warming  
33 event in comparison with other events. Note, that the shown changes remain in the 70-80 km range while Funke  
34 et al. (2009) reports on effects down to 30 km for the 2004 major warming event. Such a three-dimensional  
35 picture would allow to place the local observations into a global  
36 context.

37  
38 **AC: Comparison with MLS data is now included (Figure 3). This shows good agreement. We extend CO**  
39 **profiles into the stratosphere (see new Figure 3).**

40  
41 RC: 2) Explanation: The present explanation of the observed mesospheric is highly speculative. It uses analysis  
42 data for the stratosphere which does not directly imply a clear picture of the mesosphere. So you can not use the  
43 presence of stratospheric planetary waves to explain oscillations in the mesosphere on the daily basis. For such a  
44 link mesospheric data are required, which exist with satellites.

45  
46 **AC: Satellite mesospheric data from MLS is now included for explanation in a new text in Sect. 4.1, 4.3,**  
47 **4.4 and Supplement.**

49 In this sense, you give some information on MLS-derived temperatures in figures 2.a and 7, but the latter is very  
50 noisy and not very helpful. The presentation of maps at selected levels would considerably help the  
51 interpretation of local CO and T observations in terms of three-dimensional transports.

52  
53 **AC: Maps of the CO distribution at selected level have been created and they are described in new Sect.**  
54 **4.1 (Figure 4, Figure S1 and Figure S2). Along with CO profiles (Figure 3) they are used for the CO**  
55 **motion analysis in terms of horizontal and vertical transports.**

56  
57 RC: 3) Concentration: In some points the discussion of stratospheric dynamics is distracting the reader. Given  
58 the aim of the paper to present and understand the local mesospheric CO behavior, the detailed presentation of  
59 stratospheric circulation patterns in figures 3, 5 and 6 and related texts does not help this understanding and  
60 should be erased in favor of a concise discussion of joint stratosphere-mesosphere data in the sense of the  
61 comment above.

62  
63 **AC: Figures 3, 5 and 6, and the discussion of stratospheric dynamics has been erased.**

64  
65 RC: TECHNICAL CORRECTIONS

66  
67 L19: Change "was" to "is" for present tense. [Corrected](#)

68 L23: Change "have been" to "are". [Corrected](#)

69 L42: Change "happened" to "happens". [Corrected](#)

70 L45: Change "The" to "A". [Corrected](#)

71 L51: Insert "is" after "database". [Corrected in L53.](#)

72 L56: Replace "waves" by "activity" and "propagate" by "propagates" [Corrected in L60.](#)

73 L58: What do you mean with "upward transfer of the momentum and heat"? The EP flux is the flux of wave  
74 activity, which is much upward and equatorward in the case of SSWs. Please, reformulate. [AC: Old Figure 2](#)  
75 [and corresponding text have been removed.](#)

76 L61: Insert "its" after "is". [Corrected in L64.](#)

77 L65: Change "atmosphere" to "atmospheric". [Corrected in L68.](#)

78 L84: Replace "in" with "associated with", for example. [Replaced in L94.](#)

79 L143: Replace "are" with "is" because it refers to "data set" (singular). [Corrected in L152.](#)

80 L156: Insert a comma after "snow". [Inserted in L166.](#)

81 L160: Why not use "CO" for "carbon dioxide" (here and elsewhere)? [Corrected in L169 and hereinafter.](#)

82 L161: Are these validation tests published and documented? Please, provide a reference. [Reference provided in](#)  
83 [L170.](#)

84 L162: Why not use "MWR" for "microwave radiometer" (here and elsewhere)? [Corrected in L174 and](#)  
85 [hereinafter.](#)

86 L166: Above you wrote "sideband" - please, unify. [Corrected in L174.](#)

87 L167: Replace "The first" with "At first". [L175: Corrected to "Firstly" as proposed by Referee #2.](#)

88 L169: Replace "The second" with "At second". [L177: Corrected to "Secondly" as proposed by Referee #2.](#)

89 L175: Which of the two methods were used for this article?

90 [AC: Explained in L182–184. In this article, the both methods were used with averaging the values of the zonal](#)  
91 [wind speed for altitudes of 70–85 km. Time interval January 1 – March 31, 2018 including the SSW 2018 event](#)  
92 [is considered.](#)

93 L178: What do you mean with "similar"? Rügenachts instrument is for ozone at 30-79  
94 km - please, specify yours.

95 [AC: This paragraph has been removed.](#)

96 L185: Insert "and" before "have". [Inserted in L191.](#)

97 L200: Shorten subtitle to "3 Northern hemisphere SSW effects" in the same style as

98 for section 4. [Shortened, L210.](#)  
99 L202: Begin with "The general" and insert "a" after "is". [Sentence rephrased in L212.](#)  
100 L204: Insert "a" before "sequence". [Inserted and rephrased in L214.](#)  
101 L212: Why not use "SSW" for "sudden stratospheric warming" (here and elsewhere)?  
102 [AC: We use "SSW" in L227 and below.](#)  
103 L225: Replace "in the" with "into". [Sentence rephrased in L229–230.](#)  
104 L233: See comment for L58.  
105 [AC: The text corrected. The EP-flux discussion removed.](#)  
106 L238: Replace "since" with "after". [The text removed.](#)  
107 L242: "QBO" appears only once in the text, so it does not indeed to be abbreviated. [The text removed.](#)  
108 L244: Insert "less likely" after "latitudes". [The text removed.](#)  
109 L256: Correct "WMR" to "VMR". [Corrected in L256.](#)  
110 L376: Insert "The" before "Elevation". [This paragraph has been removed.](#)  
111 L377: Insert "A" before "Similar". [This paragraph has been removed.](#)  
112 L437: The paragraph should be shifted to where first reference to Fig. 4 is made. [This paragraph has been](#)  
113 [removed.](#)  
114 Fig.2: Please, mark "10 Feb" in (a) as in (b),(c), and (d). [Corrected in all Figures.](#)  
115 Fig. 4: Please, indicate height ranges in (a) and (b) as in (c) and (d). [Corrected, indicated in new Figure 3.](#)  
116 Fig. 7: Please, indicate "10 Feb" as in Fig. 2. [Corrected in all Figures.](#)

117  
118  
119  
120

## 121 **Reply to Referee #2**

122

123 Ref: Atmos. Chem. Phys. Discuss., <https://doi.org/10.5194/acp-2018-1361-RC2>, Mar 16, 2019  
124 Title: "Winter 2018 major sudden stratospheric warming impact on midlatitude mesosphere from microwave  
125 radiometer measurements" by Yuke Wang et al.

126

127 [We thank Referee #2 for useful comments, discussion and proposals for corrections. We made corrections and](#)  
128 [changed the text according suggestions. Our revisions and reply to Referee #2 comments are below in blue](#)  
129 [colored text. RC \(AC\) is Referee \(Authors\) comments. Line numbers of the revised manuscript are indicated.](#)

130

## 131 **Referee #2 Comments:**

132 General comment:

133

134 **RC:** This study used the reanalysis and microwave radiometer measurements to investigate the February 2018  
135 SSW event and its impact on the midlatitude mesosphere from an in-situ site. Given that the application of  
136 radiometers measurements into the SSW studies is still lack, this manuscript is suitable for the Atmospheric  
137 Chemistry and Physics journal. However, I have a concern about the novelty of the paper.

138 The SSW events, their impacts, and predictions have been widely explored in literature, but this study shows  
139 little review on the previous studies (e.g., Charlton et al. 2007JC; Hu, Ren, et al. 2014JAS; Taguchi 2018JGR;  
140 Rao et al. 2018JGR; Tripathi et al. 2016MWR; Karpechko et al. 2018GRL; Rao et al. 2019AAS). By comparing  
141 the previous studies and this one, the novelty of this study can be well stressed in the introduction and  
142 discussion sections. The authors are responsible for their investigating the latest publications about this topic on  
143 their own. In addition, some typos and description errors still exist in the manuscript. The structure of this  
144 version can be further improved. Therefore, I recommend a major-plus revision. If those problems are well  
145 solved, the ACP journal can consider its publication. Please see my specific comments below.

146

147 [AC: We \(i\) added new results in the revised manuscript \(Fig. 3, Fig. 4, Figs. 6–9 and Supplemental](#)  
148 [Material\), \(ii\) better structured Sections of the results and discussion, \(iii\) highlighted the novelty and \(iv\)](#)  
149 [corrected typos and errors.](#)

150

151 Major comments:  
152 **RC1.** The **English language** needs to be further improved. Many weird expressions can be found in this  
153 manuscript. I will list all of them in the minor comments one by one. I found some English speakers in the  
154 coauthors. Send this manuscript to all of them and well **polish the language** and correct all typos.

155  
156 **AC1: We have improved the grammar in the manuscript and corrected errors.**

157  
158 **RC2.** The organization of the manuscript is disappointing. I found many data links in the main body of the  
159 "paper" (Lines 236, 243, 415, 741, 743, 748, 779 : : : : :). Why not introduce all the datasets in the method  
160 section? Or present a table to list all the data sources the authors used. The random placement of any dataset  
161 largely diminishes the general quality of the manuscript. The authors are writing a scientific article, not a diary.

162  
163 **AC2: We have moved description of the data sets to sub-Section 2.2 and, partially, to Supplement.**

164  
165 **RC3.** The discussion section seems to be a replication of the former sections, not a real discussion at all. The  
166 authors need to compare their result with others (e.g., Taguchi 2018; Karpechko et al. 2018; Rao et al. 2019: : :  
167 : :) to put an emphasis on the new finding of the study. Another concern is about the discussion on the  
168 stratopause elevation, descent, and disappearance, which are not shown in any figure. If the stratopause is  
169 drawn in relevant figures (Figs. 2, 4 and 6), their description will be more easily understood.

170  
171 **AC3: We have improved the structure of the discussion (new sub-Sections 5.1–5.3 have been introduced)**  
172 **and conclusions as suggested.**

173  
174 **RC4.** Some low-level mistakes should be avoided as much as possible. For example, it is well known that the  
175 ERA Interim has 37 levels from 1000 hPa to 1 hPa (Dee et al, 2011), but the authors can extend this reanalysis  
176 to 0.01 hPa (Line 188) and 0.1 hPa (Line 196). They did not refer to ERA Interim website for accurate  
177 introduction, but did to the second-hand data source (Line 197). Where is the 60-layer ERA Interim (Line 196)  
178 dataset from? Similar problems can also be found in other data sources. Please carefully check, check and  
179 recheck, and search, search and re-search. The authors should make sure that they present a real research.

180  
181 **AC4: We have corrected the specific errors and omissions noted above, and made other improvements**  
182 **for consistency. Details of the pressure level ranges are described in Supplemental Section “The**  
183 **description of the data used for analysis”.**

184  
185  
186 Minor comments:

187 RC1. L22: ERA Interim, NCEP/NCAR, and other second-hand datasets that have been processed by others.  
188 Right?

189 **AC1: L22 corrected to “Data from the ERA-Interim and MERRA-2 reanalyses,...”. Other data sources are**  
190 **described in Section 2.2.**

191 RC2. L23: reanalyzes => reanalyses.

192 **AC2: Corrected in L22.**

193 RC3. L42: Awkward expression for "the event of SSW" => the SSW event.

194 **AC3: L42 Corrected to “Major sudden stratospheric warming (SSW) events which happen roughly...”**

195 RC4. L46, L49: Weird phrase for "eastward", "westward"=> westerlies, easterlies.

196 **AC4: Corrected throughout the manuscript.**

197 RC5. L51: The citations are not exhaustive. Other studies should be well reviewed.

198 **AC5: Other studies cited in L47–53.**

199 RC6. L52-55: Weird transition for the topics. What is the "usefull tool"? Can you provide more information for  
200 readers?

201 **AC6: More information is provided in L57–59.**

202 RC7. L58-59: The explanation is wrong. The upward propagations of waves do not denote the upward  
203 propagation of momentum and heat. The EP flux components are nearly proportional to the eddy momentum  
204 flux and eddy heat flux, so the poleward eddy heat flux favors the polar warming. It is wrong to stress the  
205 upward transfer of heat.

206 **AC7: L62–63, the text corrected to “The enhanced wave activity results in the rapid warming of the polar**  
207 **stratosphere and the breakdown of the stratospheric polar vortex...”**

208 RC8. L61: ": : : is impact : : ." => is its impact .  
209 [AC: Corrected in L64.](#)  
210 RC9. L63: "during the weeks or even month" =>in weeks or even more than one month  
211 [AC9: L66, corrected to “during the following weeks to month”.](#)  
212 RC10. L72: upward displacements or downward displacements?  
213 [AC10: Detailed in L75–80.](#)  
214 RC11. L89-90: Are you sure de la Torre et al. (2012) developed the WACCM and Shepherd et al. (2014)  
215 developed the CMAM. If they are the model users, please rephrase.  
216 [AC11: L98–100, The text rewritten.](#)  
217 RC12. L92: for example=> e.g.  
218 [AC12: Corrected in L102.](#)  
219 RC13. L99: exchange in stratosphere-mesosphere coupling => exchange between the stratosphere and the  
220 mesosphere?  
221 [AC13: Corrected in L108–109.](#)  
222 RC14. L101: the => a  
223 [AC14: Corrected in L110.](#)  
224 RC15. L111-112: Use the past tense.  
225 [AC15: Corrected in L119–120.](#)  
226 RC16. L127: change "sub-vortices" to "sister vortices."  
227 [AC16: Changed in L136.](#)  
228 RC17. L128: Few articles use "eastward" and "westward" to denote the zonal wind direction. The wind  
229 direction refers to where the wind comes from, not where the wind will go. Did the authors learn some lessons  
230 like an introduction to meteorology?  
231 [AC17: Corrected to “westerly” and “easterly” throughout the text.](#)  
232 RC18. L130-L132: It is not true. Rao et al. (2018) first reported the February 2018 SSW, followed by  
233 Karpechko et al. (2018), right?  
234 [AC18: Corrected to \(Rao et al., 2018; Karpechko et al., 2018; Vargin and Kiryushov, 2019\) in L138.](#)  
235 RC19. L133: Use the present tense.  
236 [AC19: Corrected, L143.](#)  
237 RC20. L143: in the 2017/18 winter?  
238 [AC20: Corrected, L153.](#)  
239 RC21. L144: Weird expression. Consider? Please rephrase.  
240 [AC21: Rephrased, L152–153.](#)  
241 RC22. L145: What does "this" refer to?  
242 [AC22: Removed, L153.](#)  
243 RC23. L152: You think midlatitudes are in Kharkiv? It will be better to change to "Kharkiv in midlatitudes".  
244 [AC23: Changed, L162.](#)  
245 RC24. L159: Please check the ACP citation format. "Pidyachiy et al. 2010; Pidyachiy et al. 2017"=>  
246 Pidyachiy et al. 2010, 2017  
247 [AC24: Corrected, L168.](#)  
248 RC25. L160: Delete "observations".  
249 [AC25: Rewritten, L169.](#)  
250 RC26. L162: Wrong citation format.  
251 [AC26: Corrected, L170.](#)  
252 RC27. L167, 169: The first, the second=> Firstly, secondly.  
253 [AC27: Corrected, L175, L177.](#)  
254 RC28. L168: by search : : :=> by searching  
255 [AC28: Corrected, L176.](#)  
256 RC29. L178: similar to=> consistent with  
257 [AC29: Rewritten, 182–184.](#)  
258 RC30. L188, L196: 0.01hPa? 0.1hPa? 60 layers?  
259 [AC30: Detailed in Supplement, page 1.](#)  
260 RC31. L190-191: Rephrase this sentence.  
261 [AC31: Changed in revised Section 2.2.](#)  
262 RC32. L202: What do you mean by "general tendency"?

263 AC32: L 212–214, corrected to: “Descending air masses are observed throughout the mesosphere and  
264 stratosphere of the winter polar region (Orsolini et al., 2010; Chandran and Collins, 2014; Limpasuvan et al.,  
265 2016; Zülicke et al., 2018).”  
266 RC33. L205: in the 2017/18 winter.  
267 AC33: Corrected, L215.  
268 RC34. L207: Why is it "enhanced warming"? It will mislead readers that the warming is enhanced. Similar  
269 problems can be also seen in Line 211.  
270 AC34: Removed in both cases, L215–217.  
271 RC35. L212: Use the present tense. Reverse=> reversal  
272 AC35: Corrected, L229.  
273 RC36. L219-220, 226: Rao et al. (2018) also studied the January 2009 SSW.  
274 AC36: Corrected, L236.  
275 RC37. L225-226: You can just say: "the SSW in February 2018 is mainly forced by wave 2"  
276 AC37: Rewritten, L229–230.  
277 RC38. L227: The description is not clear. Maybe you can describe something like this: The domination of  
278 planetary waves changes from wave 1 in January to wave 2 in February.  
279 AC38: Description improved L232–234.  
280 RC39. L230-231: This conclusion contradicts with the 2018 February SSW type. The vortex split SSW events  
281 are mainly caused by the wave 2. If you diagnose the poleward eddy heat flux at 100 hPa, you will not reach  
282 such conclusion.  
283 AC39: This fragment has been removed.  
284 RC40. L232: Delete "vector".  
285 AC40: This paragraph has been removed.  
286 RC41. L233-234: This expression is wrong. The EP flux is parallel to the planetary wave propagation, but  
287 cannot measure the upward transfer of heat flux and momentum flux. The eddy heat flux ( $[T'v']$ ) and eddy  
288 momentum fluxes ( $[u'v']$ ) are a good measure of meridional transport, NOT VERTICAL transport.  
289 AC41: This paragraph has been removed. The detailed study of EP flux behavior during the event left for future  
290 consideration.  
291 RC42. L235: The EP flux is a second-hand product based on NCEP/NCAR reanalysis and redistributed by  
292 ESRL. The data should be introduced in the method section. If the authors calculate the EP flux themselves, the  
293 procedure should also be described.  
294 AC42: This paragraph has been removed.  
295 RC43. L241: I draw the QBO evolution based on NCEP/NCAR reanalysis and do not find the same conclusion  
296 as the authors obtained. Moreover, if the QBO is in its easterly phase, the equatorward transport of waves is  
297 suppressed (Holton and Tan 1980). The authors are responsible for their correct explanation of their results.  
298 AC43: The results related to EP-flux have been removed.  
299 RC44. L260: What does the 6-ppmb level mean? I guess the authors mean the 6-ppmb contour. Moreover, the  
300 figure caption does not depict the white contour. Add the caption for the white contours and delete "(thin parts :  
301 : :: : :)"  
302 AC44: Corrected, L260, L263. Figure 3 caption updated, "thin parts..." deleted.  
303 RC45. L265: Change the citation format. It will be better to revise to "[Fig. 4 in Koo et al. (2017); Fig. 5 in  
304 Rayan et al. (2017)]"  
305 AC45: Corrected, L267–268.  
306 RC46. L269: I can not understand why the authors used weird phase like "eastward direction". What if you just  
307 use "westerly winds"?  
308 AC46: Corrected to “westerly wind” throughout the manuscript.  
309 RC47. L278: Have you compared the effects of the February 2018 SSW event in different regions? If not, how  
310 can you get such conclusion?  
311 AC47: Corrected, L253–255, and Fig. 4 is introduced for illustration.  
312 RC48. L284: What is "this Z"? Do you have "that Z"? Revised to "The Z : : :"  
313 AC48: This fragment has been removed.  
314 RC49. L285: What do you mean by "that"?  
315 AC49: This paragraph has been deleted.  
316 RC50. L291-294: This long sentence is not easy to understand. Please split and rephrase.  
317 AC50: This paragraph has been deleted  
318 RC51. L299-300: Did you perform a power spectra analysis? The authors mentioned the "5-8 days period".  
319 AC51: Spectral analysis provided and results included in new Section 4.4.

320 RC53. L302: What are the atmospheric normal modes?  
321 [AC53: This paragraph has been removed.](#)  
322 RC54. L308: the easterly winds.  
323 [AC54: This paragraph has been removed.](#)  
324 RC55. L313: What are the "reverse process"?  
325 [AC55: This paragraph has been removed.](#)  
326 RC56. L316: What are the "meridional tendency"?  
327 [AC56: This paragraph has been removed.](#)  
328 RC57. L328: I found that the authors did not know where they should put the adverb "also". Please shift it after  
329 "are". Revise throughout the manuscript.  
330 [AC57: Corrected.](#)  
331 RC58. L334: Relative to what the influence weakens?  
332 [AC58: Old Fig. 6 and related text have been removed.](#)  
333 RC59. Section 5: This section is result indeed, not a real discussion. Please add more discussion on the  
334 differences between this study and previous studies (Rao et al. 2018JGR; Karpechko et al. 2018GRL : : : : :).  
335 Emphasize the novelty of your work.  
336 [AC59. Discussion has been updated; see new Section 5 and sub-Sections 5.1–5.3.](#)  
337 RC60. L341: westward : : : wind => mesospheric easterly winds  
338 [AC60: Corrected and rewritten in L433, see AC61.](#)  
339 RC61. L342: Only wind speed? I don't think so.  
340 [AC61: The CO altitude profiles in the mesosphere have been measured by the MWR with one day time](#)  
341 [resolution. Using the CO molecule as tracer, the wind speed has been retrieved from the Doppler shift of the CO](#)  
342 [115.3 GHz emission and the mesospheric winds reverse from westerly to easterly below the winter mesopause](#)  
343 [region \(70–85 km\) has been detected. L431–434](#)  
344 RC62. L345–346: Replicate the method. Is there any new information?  
345 [AC62: Sentence rephrased in L431–434.](#)  
346 RC63. L348: Reanalyzes (verb) => reanalyses (noun)  
347 [AC63: Corrected in L438.](#)  
348 RC64. L355, L456: The stratopause variation was not explored at all. How did the authors come to the  
349 conclusion on "stratopause disappearance"?  
350 [AC64: The stratopause variations are described in new Section 4.3.](#)  
351 RC65. L357: Ambiguous phrase "increase in winter season".  
352 [AC65: Deleted.](#)  
353 RC66. L369: What is "the similar processes"? Rather ambiguous.  
354 [AC66: Removed.](#)  
355 RC67. L372: "This Z" => "The : : :"  
356 [AC67: Removed.](#)  
357 RC68. L378: Who noted this? Could you add a citation?  
358 [AC68: Removed.](#)  
359 RC69. L387: Delete "meridian".  
360 [AC69: Deleted. The changes in the CO field are illustrated in new Fig. 4, Fig. S1 and S2 and are described in](#)  
361 [related text.](#)  
362 RC70. L389: Did you show this?  
363 [AC70: The results to confirm this are included in new Section 4.1 and are discussed in Section 5.1.](#)  
364 RC71. L400: Did you mean the blocking high?  
365 [AC71: Removed. Analysis is focused on the CO re-distribution at different pressure levels in the context of the](#)  
366 [wave effects \(Sections 4.1 and 5.1\).](#)  
367 RC72. L404–406: Rephrase this sentence.  
368 [AC72: Removed.](#)  
369 RC73. L407: again? How many replacements of warming by cooling happened?  
370 [AC73: Rephrased in L522–523.](#)  
371 RC74. L414: What are the large-scale process? The authors seemed to hide some useful information. Another  
372 data link appears. The organization of the manuscript needs to be improved.  
373 [AC74: Removed. Zonal wave spectra are presented and discussed in new Sections 4.4 and 5.3.](#)  
374 RC75. L419: What do the previous studies refer to? Add the citations directly.  
375 [AC75: Citation added in L572–575.](#)  
376 RC76. L435: Add a comma after "(2012)" and after "(2014)".

377 [AC76: This paragraph has been rephrased in L501–509.](#)

378 RC77. L450: registered? Revised to "documented".

379 [AC77: Corrected, L603.](#)

380 RC78. L466: Add "is" after "which".

381 [AC78: Corrected in L635.](#)

382

383 [Proposed references added and discussed.](#)

384

385 References:

386 Rao, J., R.-C. Ren, H. Chen, X. Liu, Y. Yu, and Y. Yang, 2019: Subseasonal to seasonal hindcasts of  
387 stratospheric sudden warming by BCC\_CSM1.1(m): A comparison with ECMWF. *Adv. Atmos. Sci.*, accepted.  
388 doi: 10.1007/s00376-018-8165-8.

389 Charlton, A. J., and L. M. Polvani, 2007: A new look at stratospheric sudden warmings. Part I: Climatology  
390 and modeling benchmarks. *Journal of Climate*, 20, 449-469. Hu, J., Ren, R., & Xu, H. (2014). Occurrence of  
391 winter stratospheric sudden warming events and the seasonal timing of spring stratospheric final warming.  
392 *Journal of the Atmospheric Sciences*, 71(7), 2319-2334, doi:10.1175/JAS-D-13-0349.1.

393 Rao, J., R. Ren, H. Chen, Y. Yu, and Y. Zhou, 2018: The Stratospheric Sudden Warming Event in February  
394 2018 and its Prediction by a Climate System Model. *J. Geophys. Res. Atmos.*, 123(23), 13332-13345, doi:  
395 10.1029/2018JD028908.

396 Taguchi, M., 2018: Comparison of Subseasonal-to-Seasonal Model Forecasts for Major Stratospheric  
397 Sudden Warmings. *Journal of Geophysical Research: Atmospheres*, 123, 10,231-210,247,  
398 doi:10.1029/2018jd028755.

399 Karpechko, A. Y., A. Charlton-Perez, M. Balmaseda, N. Tyrrell, and F. Vitart, 2018: Predicting  
400 Sudden Stratospheric Warming 2018 and its Climate Impacts with a Multi-Model Ensemble. *Geophysical*  
401 *Research Letters*, 45, 13,538-513,546, doi:10.1029/2018gl081091.

402 Tripathi, O. P., Baldwin, M., Charlton-Perez, A., Charron, M., Cheung, J. C. H., Eckermann, S. D., Gerber,  
403 E., Jackson, D.R., Kuroda, Yu., Lang, A., McLay, J., Mizuta, R., Reynolds, C., Roff, G., Sigmond, M., Son, S.-  
404 W., and Stockdale, T. 2016. Examining the Predictability of the Stratospheric Sudden Warming of January 2013  
405 Using Multiple NWP Systems. *Monthly Weather Review*, 144, 1935-1960, doi:10.1175/mwr-d-15-0010.1.

406

407

408 [On behalf of authors](#)

409 [Gennadi Milinevsky](#)

410

411

412

413

414

415

416 [New text of manuscript:](#)

417



1 **Winter 2018 major sudden stratospheric warming impact on midlatitude mesosphere from**  
2 **microwave radiometer measurements**

3  
4 Yuke Wang<sup>1</sup>, [Valerii Shulga](#)<sup>1,2</sup>, Gennadi Milinevsky<sup>1,3</sup>, Aleksey Patoka<sup>2</sup>, Oleksandr Evtushevsky<sup>3</sup>,  
5 Andrew Klekociuk<sup>4,5</sup>, Wei Han<sup>1</sup>, Asen Grytsai<sup>3</sup>, Dmitry Shulga<sup>2</sup>, Valery Myshenko<sup>2</sup>, Oleksandr  
6 Antyufeyev<sup>2</sup>

7  
8 <sup>1</sup>College of Physics, International Center of Future Science, Jilin University, Changchun, 130012,  
9 China

10 <sup>2</sup>Institute of Radio Astronomy, NAS of Ukraine, Kharkiv, 61002, Ukraine

11 <sup>3</sup>Taras Shevchenko National University of Kyiv, Kyiv, 01601, Ukraine

12 <sup>4</sup>Antarctica and the Global System, Australian Antarctic Division, Kingston, 7050, Australia

13 <sup>5</sup>[Department of Physics, University of Adelaide, Adelaide, 5005, Australia](#)

14  
15 *Correspondence to:*

16 Gennadi Milinevsky (genmilinevsky@gmail.com) and Valerii Shulga (shulga@rian.kharkov.ua)

17  
18 **Abstract.** The impact of a major sudden stratospheric warming (SSW) in the Arctic in February 2018  
19 on the mid-latitude mesosphere [is](#) investigated by performing microwave radiometer measurements of  
20 carbon monoxide (CO) and zonal wind above Kharkiv, Ukraine (50.0°N, 36.3°E). The mesospheric  
21 peculiarities of this SSW event were observed using [a](#) recently designed and installed microwave  
22 radiometer in East Europe for the first time. [Data](#) from the ERA-Interim and [MERRA-2 reanalyses](#), as  
23 well as the Aura Microwave Limb Sounder measurements, [are](#) also used. Microwave observations of  
24 the daily CO profiles in January–March 2018 allowed [the retrieval of](#) mesospheric zonal wind at 70–  
25 85 km (below the winter mesopause) over the Kharkiv site. [Reversal](#) of the mesospheric westerly from  
26 about 10 m s<sup>-1</sup> to [an](#) easterly wind of about –10 m s<sup>-1</sup> around 10 February [was observed](#). [The](#) local  
27 microwave observations [at our](#) NH midlatitude [site](#) combined with reanalysis data show wide [ranging](#)  
28 daily variability in CO, zonal wind [and](#) temperature in the mesosphere and stratosphere during the  
29 SSW [of](#) 2018. The observed [local](#) CO variability can be explained [mainly](#) by horizontal air mass  
30 redistribution due to planetary wave activity. Replacement of the CO-rich [polar vortex](#) air by CO-poor  
31 air [of the surrounding area](#) led to a significant mesospheric CO decrease over the station during the  
32 SSW and fragmentation of the vortex over the station at the SSW start caused enhanced stratospheric  
33 CO at about 30 km. Spectral analysis shows intensified westward wave 1 throughout the midlatitude  
34 upper stratosphere–mesosphere, consistent with other studies of SSWs in the NH winter polar region.  
35 The results of microwave measurements of CO and zonal wind in the midlatitude mesosphere at 70–85

36 km altitudes, which still is not adequately covered by ground-based observations, are useful for  
37 improving our understanding of the SSW impacts in this region.

38

39

## 40 **1 Introduction**

41

42 Major sudden stratospheric warming (SSW) events which happen roughly each two years in the North  
43 Polar region are produced by strong planetary wave activity according to the model developed by  
44 Matsuno (1971) which is supported by numerous observations (Alexander and Shepherd, 2010;  
45 Kuttippurath and Nikulin, 2012; Tao et al., 2015). A major SSW event is accompanied by a sharp  
46 increase of the stratosphere temperature up to 50 K and the reversal of the zonal wind from  
47 climatological westerlies to easterlies over a period of several days (Charlton and Polvani, 2007;  
48 Chandran and Collins, 2014; Hu et al., 2014; Tripathi et al., 2016; Butler et al., 2017; Karpechko et al.,  
49 2018; Taguchi, 2018; Rao et al., 2018). The primary definition of a SSW event provided by the World  
50 Meteorological Organization requires a stratosphere temperature increase and an accompanying zonal  
51 wind reversal to easterlies at the 10-hPa pressure level (approximately 30 km altitude) and 60° latitude  
52 (WMO, 1978). This definition was broadened and detailed in recent papers (Butler et al., 2015; Butler  
53 and Gerber, 2018; Rao et al., 2019). The summarizing paper, where a SSW database is described, was  
54 published in Butler et al. (2017). This useful tool  
55 (<https://www.esrl.noaa.gov/csd/groups/csd8/sswcompendium/>) allows analysis of the conditions in the  
56 stratosphere, troposphere, and at the surface before, during and after each SSW event representing its  
57 evolution, structure, and impact on winter surface climate. The compendium is based on data from six  
58 different reanalysis products, covers the 1958–2014 period and includes global daily anomaly fields,  
59 full fields, and derived products for each SSW event (Butler et al., 2017).

60 The source of the SSW is planetary wave activity born in the troposphere that propagates upward  
61 through the tropopause to the stratosphere (Matsuno, 1971; Alexander and Shepherd, 2010, Butler et  
62 al., 2015). The enhanced wave activity results in the rapid warming of the polar stratosphere and the  
63 breakdown of the stratospheric polar vortex (Matsuno, 1971; de la Torre et al., 2012; Chandran and  
64 Collins, 2014; Pedatella et al., 2018). The important feature of a SSW event is its impact on lower  
65 altitudes, when temperature and wind anomalies descend downward into the high- and mid-latitude  
66 troposphere during the following weeks to month and influence the surface weather (Baldwin and  
67 Dunkerton, 2001; Zhou et al., 2002; Butler et al., 2015; Yu et al., 2018). The major SSW events may  
68 also impact the atmospheric composition of the whole Northern Hemisphere (NH) stratosphere  
69 including mid-latitudes (Solomon et al., 1985; Allen et al., 1999; Tao et al., 2015).

70 During the SSW, vertical coupling covers not only the troposphere but extends upward to the  
71 mesosphere. Mesospheric responses to the SSW are observed as enhancement in planetary wave  
72 amplitude, zonal wind reversal and significant air cooling (Shepherd et al., 2014; Zülicke and Becker,  
73 2013; Stray et al., 2015; Zülicke et al., 2018), substantial depletion of the metal layers (Feng et al.,  
74 2017; Gardner, 2018), mesosphere-to-stratosphere descent of trace species (Manney et al., 2009; Salmi  
75 et al., 2011). The SSW events are also accompanied by the rapid descent of the stratopause into the  
76 stratosphere at the SSW onset, following formation of the elevated stratopause in the lower  
77 mesosphere and gradual stratopause lowering toward its typical position in the SSW recovery phase  
78 (Manney et al., 2009; Chandran et al., 2011; Salmi et al., 2011; Tomikawa et al., 2012; Limpasuvan et  
79 al., 2016; Orsolini et al., 2010, 2017). The elevated stratopause events provide an evidence of the  
80 coupling between the stratosphere and the mesosphere.

81 Among the trace gases, the CO molecule is a good tracer of winter polar vortex dynamics in the  
82 upper stratosphere and mesosphere due to its long photochemical lifetime (Solomon et al., 1985; Allen  
83 et al., 1999; Rinsland et al., 1999, Shepherd et al. 2014). The CO mixing ratio generally increases with  
84 height in the upper stratosphere and mesosphere and increases with latitude toward the winter pole.  
85 This is due to the mean meridional circulation which transports CO from the source region in the  
86 summer hemisphere and tropics to the extratropical winter mesosphere and stratosphere (Shepherd et  
87 al., 2014). Therefore, large abundances of CO appear in the winter polar regions under conditions of  
88 large-scale planetary wave activity. Downward meridional transport causes descent of CO between the  
89 mesosphere and stratosphere and this process is sensitive to planetary wave amplitudes, and  
90 particularly the wave amplitude changes that occur during SSWs (Rinsland et al., 1999; Manney et al.,  
91 2009; Kvissel et al., 2012). Due to the large scale descent, high CO values of mesospheric origin are  
92 observed at stratospheric altitudes down to 25–30 km (Engel et al., 2006; Huret et al., 2006; Funke et  
93 al., 2009). At NH mid-latitudes, CO also exhibits significant variability during periods of planetary  
94 wave activity associated with SSWs, when the polar vortex splits and displaces off the pole (Solomon  
95 et al., 1985; Allen et al., 1999; Funke et al., 2009).

96 Recent atmospheric models are being extended up to 80–150 km and are used for the study of  
97 SSWs (de la Torre et al., 2012; Chandran and Collins, 2014; Shepherd et al., 2014; Limpasuvan et al.,  
98 2016; Newnham et al., 2016). For example, de la Torre et al. (2012) applied the Whole Atmosphere  
99 Community Climate Model (WACCM) and Shepherd et al. (2014) used the Canadian Middle  
100 Atmosphere Model (CMAM) for SSW modeling. The reference wind profiles for the models are  
101 mainly retrieved from observations of the radiation of the mesospheric ozone molecules, which allow  
102 robust measurements at altitudes up to of approximately 65 km (e.g., Hagen et al., 2018). These data  
103 are generally consistent with the most commonly used reanalysis products. However, there are still  
104 insufficient observations of middle atmospheric winds at altitudes between 60 and 85 km made with a

105 high vertical resolution to verify atmospheric models and possible long-term trends (Keuer et al., 2007;  
106 Hagen et al., 2018; Rüfenacht et al., 2018). This altitude range, where temperature generally decreases  
107 with height which causes inherent vertical instability, is situated below the winter mesopause region at  
108 95–100 km (e.g. Xu et al., 2009) and plays a significant role in the mass and energy exchange between  
109 the stratosphere and the mesosphere (Shepherd et al., 2014; Limpasuvan et al., 2016; Gardner, 2018).

110 Microwave radiometry is a ground-based technique that can provide vertical profiles of CO, H<sub>2</sub>O  
111 and O<sub>3</sub> atmospheric gases and wind data in the upper stratosphere and mesosphere (Rüfenacht et al.,  
112 2012; Scheiben et al., 2012; Forkman et al., 2016). The upper stratosphere–mesosphere zonal winds at  
113 the 30–85 km altitude region can be measured using the Doppler shift between different observation  
114 directions in simultaneously measured spectra of transitions lines of carbon monoxide at 115.3 GHz  
115 and ozone O<sub>3</sub> at 110.8 GHz (Rüfenacht et al., 2012; Forkman et al., 2016). Due to high altitude CO  
116 residence region, the simultaneous zonal wind measurements using both O<sub>3</sub> and CO provide  
117 independent data that extend the wind measurement from the stratospheric to mesospheric altitudes,  
118 respectively (Forkman et al., 2016; Pidyyachiy et al., 2017).

119 The first ground-based microwave measurements of CO were made in the 1970s and they  
120 confirmed theoretical estimations of the vertical CO profile (Waters et al., 1976; Goldsmith et al.,  
121 1979). Since the 1990s, the ground-based microwave radiometers measuring CO have been installed in  
122 the Northern Hemisphere at high and middle latitudes to provide measurements on a regular basis.  
123 Microwave radiometers are operating in Onsala and Kiruna, Sweden, since 2008. The results are  
124 described in Hoffmann et al. (2011) and in Forkman et al. (2012). The microwave radiometer operated  
125 in Bern, Switzerland since 2010 aims to contribute to the significant gap that exists in the middle  
126 atmosphere between 40 and 70 km altitude for wind data (Rüfenacht et al., 2012). In the Arctic, the O<sub>3</sub>,  
127 N<sub>2</sub>O, HNO<sub>3</sub>, and CO spectra were recorded using the Ground-Based Millimetre-wave Spectrometer  
128 GBMS (Muscari et al., 2007; Di Biagio et al., 2010).

129 Since 2014, the microwave measuring system for CO observations has been operated in Kharkiv,  
130 Ukraine (Pidyyachiy et al., 2010; Pidyyachiy et al., 2017). Microwave radiometer measurements of  
131 CO are used to retrieve mesospheric winds nearby the mesopause region (70–85 km). Methods  
132 deriving the wind speed from mesospheric CO measurements are based on the determination of the  
133 CO and O<sub>3</sub> lines emission Doppler shift (Eriksson et al., 2011; Hagen et al., 2018).

134 Our observations in February 2018 using the new microwave radiometer at the mid-latitude  
135 Kharkiv station have recorded the mesospheric effects of a major SSW. In mid-February 2018, the  
136 stratospheric polar vortex in the Arctic splitted into two sister vortices (Fig. 1), the zonal wind reversed  
137 in the stratosphere–mesosphere from westerly to easterly and warm air penetrated into the polar cap  
138 regions (Rao et al., 2018; Karpechko et al., 2018; Vargin and Kiryushov, 2019). This caused large-  
139 scale disturbances in the middle atmosphere of the polar and middle latitudes. The major SSW in 2018

140 is not yet widely discussed in publications (Rao et al., 2018; Karpechko et al., 2018; Vargin and  
141 Kiryushov, 2019) and in this paper, we give a detailed description of the observed mesospheric CO  
142 and zonal wind variations.

143 In Sect. 2, the microwave radiometer and data processing software are briefly described. The SSW  
144 event in February 2018 is considered in Sect. 3. The effects of the SSW on mid-latitude mesosphere–  
145 stratosphere conditions in the Ukraine longitudinal sector are presented in Sect. 4. Discussion is given  
146 in Sect. 5 followed by conclusions in Sect. 6.

147

148

## 149 **2 Data and methods**

150

151 The microwave radiometer data set registered during the 2017/2018 winter campaign in Kharkiv  
152 (50.0°N, 36.3°E) is used in this study to investigate local effects of the winter 2018 sudden  
153 stratospheric warming on the mesosphere and stratosphere. Since the ground-based microwave  
154 measurements are spatially limited by instrument coverage, data on air temperature, zonal wind,  
155 geopotential height were used from reanalyses and satellite databases to interpret the CO profile and  
156 the zonal wind microwave observations and to describe the SSW effects in the atmosphere of the  
157 surrounding mid-latitude region (30–40°E, 48–52°N).

158

159

### 160 **2.1 Microwave radiometer, method, and midlatitude data description**

161

162 The microwave radiometer (MWR) with high sensitivity, installed at Kharkiv, Ukraine, is designed for  
163 continuous observations of the atmospheric CO profiles and zonal wind speed in the mesosphere using  
164 emission lines at 115.3 GHz. The radiometer can continuously provide vertical profiles up to the  
165 mesopause region during day and night, even in cloudy conditions (Hagen et al., 2018). However,  
166 precipitation, such as strong rain or snow, can prevent the measurements.

167 The receiver of the radiometer has the double-sideband noise temperature of 250 K at an ambient  
168 temperature of 10°C (Pidtyachiy et al., 2010; 2017). The radiometer was tested during the 2014–2015  
169 period for observation of the CO emission lines in the mesosphere over Kharkiv. These tests proved  
170 the reliability of the receiver system, on which further details are provided in Pidtyachiy et al. (2017).  
171 Since 2015, the radiometer has been used for continuous microwave measurements of CO profiles and  
172 mesosphere wind investigations. The first observations of the atmospheric CO spectral lines over  
173 Kharkiv have confirmed seasonal variations in the CO abundance (Pidtyachiy et al., 2017). Operation  
174 of the MWR in a double-sideband mode allows retrieval of wind speed from the Doppler shift of the

175 CO line emission at the 115.3 GHz. Two methods are used to determine wind speed. **Firstly** the  
176 observed line shape is fitted by a Voigt profile **and the center frequency is determined** (Pidyachiy et  
177 al., 2017). **Secondly** radiative transfer calculations for a horizontally layered atmosphere are used to  
178 determine the wind profiles with the Qpack package, version 1.0.93 (Eriksson et al., 2005; Eriksson et.  
179 al., 2011), which is specifically designed to work with the forward model of the Atmospheric  
180 Radiative Transfer Simulator ARTS (Buehler et al., 2018; <http://www.radiativetransfer.org/>). The  
181 results obtained by both methods were almost the same within the error limits. **In this paper, both**  
182 **methods were used and provided average values of the zonal wind speed for altitudes of 70–85 km.**  
183 **The time interval of the data used here was January 1 – March 31, 2018, which covers the main phases**  
184 **of the SSW 2018 event.**

185

186

## 187 **2.2 Data from other sources**

188

189 In this study, daily datasets from ERA-Interim global atmospheric reanalysis of European Centre for  
190 Medium-Range Weather Forecast (ECMWF; Dee et al., 2011) were downloaded from  
191 (<https://www.ecmwf.int/en/forecasts/datasets/archive-datasets/reanalysis-datasets/era-interim>) **and**  
192 have been used for comparison with MWR observations. The ERA-Interim data were used to create  
193 temperature and zonal wind velocity profiles and to calculate geopotential height at the stratospheric  
194 pressure levels, in order to compare with the data measured over **the** Kharkiv site. Aura Microwave  
195 Limb Sounder (MLS) measurements of the air temperature were analyzed as well (Xu et al., 2009;  
196 <https://mls.jpl.nasa.gov/data/readers.php>; see details in the Supplement).

197 Zonal wave amplitudes in geopotential height were analyzed using the National Oceanic and  
198 Atmospheric Administration National Centers for Environmental Prediction, Global Data Assimilation  
199 System–Climate Prediction Center (NOAA NCEP GDAS–CPC) data at  
200 <https://www.cpc.ncep.noaa.gov/products/stratosphere/strat-trop/> and the MERRA-2 data from the  
201 National Aeronautics and Space Administration Goddard Space Flight Center, Atmospheric Chemistry  
202 and Dynamics Laboratory (NASA GFC ACDL) site at [https://acd-](https://acd-ext.gsfc.nasa.gov/Data_services/met/ann_data.html)  
203 [ext.gsfc.nasa.gov/Data\\_services/met/ann\\_data.html](https://acd-ext.gsfc.nasa.gov/Data_services/met/ann_data.html). The detailed description of the data used for  
204 analysis is given in the Supplement.

205

206

207

208

209

### 210 3 Northern Hemisphere SSW effects

211

212 Descending air masses are observed throughout the mesosphere and stratosphere of the winter polar  
213 region (Orsolini et al., 2010; Chandran and Collins, 2014; Limpasuvan et al., 2016; Zülicke et al.,  
214 2018). From Aura MLS vertical profiles, a layered descending sequence of alternating cool and warm  
215 anomalies over the polar cap was observed in the 2017/2018 winter (Fig. 2a). The SSW event in Fig.  
216 2a is identified by the rapid warming in the stratosphere and cooling in the mesosphere (upward arrow)  
217 starting from 10 February 2018 (left vertical line).

218 This event was preceded by progressively descending warm and cold anomalies that formed in  
219 January (black and white dashed arrows, respectively). Oscillations in the intensity of the anomalies  
220 indicate that they were formed under the influence of large amplitude planetary waves of zonal wave  
221 numbers 1 and 2 (Fig. 2c–2e). From 1 January to 10 February (during 41 days), descending warm  
222 anomalies with a velocity  $\sim 850 \text{ m}\cdot\text{day}^{-1}$  were apparent in the mesosphere and the upper stratosphere  
223 (75 to 40 km; black dashed arrow in Fig. 2a). Below the warm anomaly, a cold anomaly descended  
224 between the upper and lower stratosphere (45 to 20 km) with velocity  $\sim 600 \text{ m}\cdot\text{day}^{-1}$  (white dashed  
225 arrow in Fig. 2a), while a cold mesospheric anomaly in February–March descended with average  
226 velocity  $\sim 750 \text{ m}\cdot\text{day}^{-1}$  (white dotted arrow in Fig. 2a). Our velocity estimates are similar to those of  
227 Salmi et al. (2011) who found that mesospheric  $\text{NO}_x$  anomalies during the major SSW 2009 were  
228 transported from 80 to 55 km in about 40 days, i.e. with velocity  $\sim 600 \text{ m}\cdot\text{day}^{-1}$ .

229 The splitting of the polar vortex (Fig. 1) and the zonal wind reversal (Fig. 2b) started at the time of  
230 the wave 2 pulse on 10 February (Fig. 2d and dashed curve in Fig. 2e). Note that this is close to the  
231 SSW timing in Rao et al. (2018) and Vargin and Kiryushov (2019), where the SSW onset date was 11  
232 February. As seen from Fig. 2c and solid curve in Fig. 2e, increasing wave 1 amplitude contributed to  
233 the destabilization of the polar vortex during January–early February and to temperature and zonal  
234 wind oscillations in the mesosphere and stratosphere (Fig. 2a and 2b). These oscillations are usually  
235 associated with the propagation of planetary waves in the stratosphere and mesosphere (Limpasuvan et  
236 al., 2016; Rüfenacht et al., 2016). As noted in an earlier study (Manney et al., 2009; Rao et al., 2018),  
237 wave 1 amplitudes were also larger prior to the SSW in 2009, suggesting a role of preconditioning.  
238 During 10–15 February, the easterly zonal wind anomaly at the stratopause (about 1 hPa,  $\sim 50$  km)  
239 increased to  $-60 \text{ m s}^{-1}$  (Fig. 2b). At the same time, warming in the polar stratosphere with the largest  
240 temperature anomaly of about 20 K was observed between 25 and 45 km in the same time interval  
241 (upward arrow in Fig. 2a). Both anomaly peaks are close in time to the wave 1 pulse after the SSW  
242 start (Fig. 2c and 2e). The descending negative temperature anomaly in the mesosphere between 50  
243 and 90 km persisted during and after the SSW and reached  $-15 \text{ K}$  (dotted arrow in Fig. 2a).

244

## 245 **4 The local SSW effects over the midlatitude station**

246

### 247 **4.1 CO variability**

248

249 Local variability in the conditions of the atmosphere during the microwave measurements in January–  
250 March 2018 at Kharkiv (50°N, 36°E) is shown in Figs. 3–6. The sharp changes occurred in the 20-day  
251 interval from 10 February to 1 March coinciding with the SSW event 2018, as indicated by red vertical  
252 lines in Figs. 3, 5 and 6. At this time the polar vortex divided into two parts producing two smaller  
253 vortices over the longitudinal sectors of North America and Eurasia (Fig. 1). Due to the planetary wave  
254 influence (Fig. 2c–2e), the two sub-vortices shifted zonally and meridionally, so that the SSW effects  
255 were observed not only in the polar region but also in the middle latitudes (Fig. 4).

256 The CO molecule volume mixing ratio (VMR) near the mesopause at 75–80 km decreased from  
257 10 ppmv of background level to 4 ppmv on 19–21 February (Fig. 3a), when the sharp vertical CO  
258 gradient at the lower edge of the CO layer near about 6 ppmv increased in height by about 8 km  
259 (between 75 km and 83 km, thick part of the white curve in Fig. 3a). For comparison, the pre- and  
260 post-SSW vertical variations of the 6-ppmv contour were observed in a range 2–3 km (white curve in  
261 Fig. 3a). Moreover, similar variations in the zonal mean 6-ppmv level are much weaker (yellow curve  
262 in Fig. 3e). This indicates that local and regional mesosphere over the MWR site was disturbed by  
263 some source acted during the SSW, which is identified below. We take here the 6-ppmv contour as a  
264 conditional lower edge of the CO layer since the CO gradients sharply increase from 0.2–0.3 ppmv  
265  $\text{km}^{-1}$  in a 10-km layer below to 0.6–0.8 ppmv  $\text{km}^{-1}$  in a 10-km layer above (below and above the white  
266 curve in Fig. 3a). The similar gradient change is characteristic of the mesospheric CO profiles in boreal  
267 winter from ground-based and satellite observations (Fig. 4 in Koo et al., 2017; Fig. 5 in Ryan et al.,  
268 2017).

269 The local mesospheric CO variability from the MWR observations over Kharkiv agrees with  
270 regional one from the MLS data averaged over the adjacent area 47.5–52.5°N, 26–46°E (Fig. 3b, the  
271 white curve for 6 ppmv). However, the zonal mean CO profiles in the same zone do not show an  
272 anomalous decrease of the mesospheric CO during the SSW (yellow curve in Fig. 3a, 3b and 3e).

273 The opposite tendency with the stratospheric CO abundance increase is observed from both  
274 regional and zonal mean MLS data shortly after the SSW start (contour 0.1 ppmv in Fig. 3d and 3g,  
275 respectively). The CO-rich air of 0.1–0.5 ppmv, which is typical for the lower mesosphere (Fig. 3c)  
276 descended up to about 30 km (Fig. 3d and 3g), far exceeding typical stratospheric CO mixing ratios on  
277 the order of about 0.01–0.02 ppmv (Engel et al., 2006; Huret et al., 2006; Funke et al. 2009). The CO-



278 rich stratospheric anomaly is close in time to the wave 1 peak on 10–15 February (solid curve in Fig.  
279 2e), that was observed through the stratosphere down to the 30 km altitude (Fig. 2c).

280 Horizontal distributions of the CO VMR in the Northern Hemisphere at the stratospheric and  
281 mesospheric altitudes in Fig. 4 explain causes of the different CO variability by vertical in Fig. 3. The  
282 dynamical deformation, elongation, and displacements relative to the pole of the polar vortex lead to  
283 temporal shifts in the low and high CO amounts over the MWR site at Kharkiv (white circle in Fig. 4).  
284 The tendency of the planetary wave westward tilt with altitude (dashed lines in Fig. 4, see also  
285 Supplemental Figs. S1 and S2 for more details) also contributes to relative zonal shift between the  
286 stratosphere and the mesosphere of the low/high CO over Kharkiv.

287 The observed decrease of the local CO in the mesosphere during the SSW (white curve in Fig. 3a)  
288 is consistent with the regional data from the satellite observations (white curve in Fig. 3b). The  
289 decrease is due to the displacement of the CO-rich air to the west relative to Kharkiv (white circle and  
290 contours outlined the CO-rich area in Fig. 4a–4c and 4e–4g). This is a result of the easterly domination  
291 during the SSW that led to placing of the CO-poor air over Kharkiv with the lowest CO levels on 19–  
292 23 February (Fig. 4c and 4g) in correspondence with the MWR (Fig. 3a) and MLS (Fig. 3b)  
293 measurements. Return to the westerly regime in early March reversed the rotation of the vortex (2–6  
294 March in Fig. 4d and 4h) and caused recovery of high CO level over Kharkiv (since about 1st of  
295 March in Fig. 3a and 3b).

296 The polar vortex split influenced the local CO change in the middle stratosphere (Fig. 4m–4o).  
297 The low CO level at ~30 km before the SSW start (Fig. 3d) is associated with the relatively distant  
298 location of the CO-rich vortex from Kharkiv (Fig. 4m). The vortex split and easterly circulation caused  
299 displacement of the small vortex fragment with the CO level higher than 0.1 ppmv to Kharkiv just at  
300 the SSW start (9–13 February in Fig. 4n) and corresponding sharp CO increase over the Kharkiv  
301 region around 30-km altitude (contour 0.1 ppmv in a few days after 10 February in Fig. 3d). Vertical  
302 CO profiles in Fig. 3c and 3d show that downward penetration of the mesospheric CO-rich air into the  
303 stratosphere took place around 10 February. As seen from Fig. 4f, 4j, and 4n, the mesospheric CO-rich  
304 air appears to be contained inside the small sub-vortex over Kharkiv. The large sub-vortex (Fig. 4n and  
305 4o) contributed to the stratospheric CO increase after 10 February in the zonal mean CO profile near  
306 30 km (Fig. 3g). The two sub-vortices in Fig. 4n and 4o provided a longer duration of the mesospheric  
307 intrusion in the zonal mean (Fig. 3g) than a short-time influence of the single sub-vortex in regional  
308 data (Fig. 3d).

309 It should be noted that the lower edge of the mid-latitude CO-rich air descended in January – mid-  
310 February (dashed lines in Fig. 3d and 3g) similarly to the temperature anomaly in the polar region (Fig.  
311 2a). Descent velocity was about -270 and -220 m·day<sup>-1</sup> in the case of the regional and zonal mean data,

312 respectively. This is a few times lower than in the vortex region, nevertheless, it is in the range of the  
313 winter descent velocity noted above (Ryan et al., 2018).

314 Note also that the vortex split in the CO distribution can be identified only in the middle and upper  
315 stratosphere (Fig. 4n and 4o and Fig. S1j and S1k), but not at the stratopause level (Fig. 4j and 4k) and  
316 in the mesosphere (Fig. S2, second and third columns for 9–13 and 19–23 February 2018,  
317 respectively).

318

319

## 320 **4.2 Zonal wind variability**

321

322 The reversal of the local zonal wind estimated from the CO measurements at the Kharkiv MWR site  
323 near the mesopause region was observed. The averaged wind velocity in the altitude range 70–85 km  
324 changed between  $10 \text{ m s}^{-1}$  and  $-10 \text{ m s}^{-1}$  around 10 February (Fig. 5a). Positive (negative) values are  
325 westerly (easterly) wind components. After the active phase of the SSW, the zonal wind returns to the  
326 westerly wind and enhances to  $20 \text{ m s}^{-1}$  reaching the highest velocity observed in January–March (Fig.  
327 5a). This zonal wind peak in early March is accompanied by the CO peak at 18 ppmv around 85 km  
328 that is also the highest CO abundance over January–March (Fig. 3a). This is closely consistent with the  
329 MLS measurements at the 86-km altitude: Kharkiv was located on the 16-ppmv contour in early  
330 March (2–6 March in Fig. 4d).

331 During the SSW event, local zonal wind over the station became easterly between the lower  
332 stratosphere and lower mesosphere ( $-30 \text{ m s}^{-1}$  up to  $-40 \text{ m s}^{-1}$ , white contours in Fig. 5b). Note that  
333 westerly zonal wind at the stratopause level ( $\sim 50 \text{ km}$ ) in January 2018 (mid-winter, the pre-SSW  
334 conditions) sometimes increased to more than  $100 \text{ m s}^{-1}$  (black contours in Fig. 5b).

335 The return of the local westerly wind in the upper mesosphere began in late February (Fig. 5a) and  
336 later, in early March, in the lower mesosphere–stratosphere (Fig. 5b). The longer persistence of the  
337 westerly anomaly in the stratosphere than at the stratopause level is seen also in the polar region (Fig.  
338 2b). This is a manifestation of the downward migration of the circulation anomalies in the SSW  
339 recovery phase, although a near-instantaneous vertical coupling is observed at the SSW start on 10  
340 February (Fig. 2a–2d and Fig. 5).

341

342

## 343 **4.3 Temperature changes**

344

345 The MLS temperature profiles show that high temperature variability over the Kharkiv region  
346 concentrated at the stratopause level, particularly before and during the SSW 2018 (Fig. 6). As known,

347 the SSW events are accompanied by polar stratopause descent to 30–40 km, by stratopause breakdown  
348 and subsequent reformation at very high altitudes of about 70–80 km (Manney et al., 2009; Chandran  
349 et al., 2011; Limpasuvan et al., 2016; Orsolini et al., 2017). The midlatitude stratopause exhibits less  
350 sharp, but significant oscillations between 40 and 50 km in January–first half of February 2018 (dotted  
351 curve in Fig. 6) and the highest temperature near  $-5^{\circ}\text{C}$  after the SSW start on 12–13 February. The  
352 short-time stratopause elevation to the lower-mesospheric altitude  $\sim 60$  km was observed near 20  
353 February, i.e. close in time to the maximum elevation of the 6-ppmv CO level in the mesosphere (Fig.  
354 3a and 3b). Note that the wave 1 and wave 2 (Fig. 2c–2e), and zonal wind (Fig. 5) do not demonstrate  
355 strong anomalies this time. The post-SSW stratopause stabilized at the 50-km altitude and warmed  
356 from about  $-20^{\circ}\text{C}$  to  $-10^{\circ}\text{C}$  (Fig. 6b).

357 Similarly to the CO profile in Fig. 3, the zonal mean temperature variability is much lower above  
358 the stratopause than the regional one (Fig. 6b and 6a, respectively). The stratosphere looks about  
359 equally disturbed in both regional and zonal mean characteristics (Fig. 3d and 3g and Fig. 6a and 6b).  
360 This difference may be associated with the influence of the splitted (non-splitted) polar vortex in the  
361 stratosphere (mesosphere). The vortex fragments introduce higher local/regional and zonal mean  
362 variability in the stratosphere; whereas the vortex region is more uniform in the mesosphere (Fig. 4).  
363 That results in the weaker zonal mean variability.

364 During the SSW, the regional stratospheric temperature in Fig. 6a was warmer by  $10\text{--}15^{\circ}\text{C}$  in  
365 comparison with the pre- and post-SSW temperature. This is about two times lower warming than in  
366 the polar region (Fig. 2a) and about three times lower than it is typically observed during the SSWs  
367 (see Section 1). It should be noted that this warm stratospheric anomaly in Fig. 6a (contour  $-55^{\circ}\text{C}$ )  
368 rapidly descended between the upper and lower stratosphere (dashed arrow) in about 10 days. A  
369 similar tendency is seen in Fig. 6b from the zonal mean (contour  $-55^{\circ}\text{C}$ ) but with a descent within a  
370 few days (arrow). So, the SSW start in the midlatitude stratosphere does not accompany by a near-  
371 instantaneous vertical coupling observed in the polar region (Fig. 2a–2d). Midlatitude stratospheric  
372 warming in February 2018 occurred with increasing time lag between the upper and lower  
373 stratosphere.

374 As is known, upward propagation of the tropospheric planetary waves into the stratosphere is  
375 limited in the easterly zonal wind (Charney and Drazin, 1961). In the changed state of a zonal flow, the  
376 critical line for planetary waves (zero wind line) in the polar region descends in a few days that looks  
377 like downward propagation of an anomaly from above (Matsuno, 1971; Zhou et al., 2002). Possibly,  
378 this process may be delayed in the midlatitude, as seen from Fig. 6.

379  
380

#### 381 4.4 Influences of zonal wave 1 and wave 2

382

383 Figure 7 shows time–longitude variations in the MLS temperature anomalies in the Kharkiv zone  
384 47.5–52.5°N with respect to the mean climatology 2005–2017. The mesospheric and stratospheric  
385 levels during January–March 2018 (Fig. 7a–7c and Fig. 7d and 7e, respectively) are presented. Dashed  
386 lines indicate a sharp change in the direction of zonal migration of the temperature anomalies from  
387 eastward to westward around 10 February. This change coincides with the reversal of the westerly to  
388 easterly at the SSW start (Fig. 2b and Fig. 5). Alternating sequences of the positive and negative  
389 anomalies in Fig. 7 indicate the planetary wave ridges and troughs migrating along the midlatitude  
390 zone.

391 In the lower–middle stratosphere (22 km in Fig. 7e, 24 and 30 km in Fig. S3h and S3i), the change  
392 in the anomaly migration direction is not as pronounced as at the upper levels. The slowly westward  
393 migrating positive anomaly is a wave 1 ridge that dominates in the eastern longitudes (black solid line  
394 in Fig. 7e and Fig. S3h–S3j). Note that the Kharkiv longitude 36°E (white line in Fig. 7 and Fig. S3)  
395 remains out of the wave 1 ridge during January–March. Wave 1 ridge weakens with altitude and wave  
396 1 trough becomes deeper in the western upper stratosphere (Fig. 7d and Fig. S3e–S3g). The vertical  
397 wave transformation is accompanied by a westward tilt with altitude seen from the sequential  
398 westward shift of both wave 1 ridge and wave 1 trough (solid and dashed lines, respectively, in Fig.  
399 S3). This tendency is consistent with the upward propagation of the planetary waves.

400 Migrating anomalies weaken rapidly after the SSW (to the right of the red vertical line on 1st of  
401 March in Fig. 7) as a result of the general decrease in wave activity (Fig. 2e). The results of Fig. 7 and  
402 Fig. S3 suggest modification of the zonal wave spectra in time and altitude and Fig. 8 and Fig. 9  
403 present the zonal wave spectra in the lower–middle stratosphere and upper stratosphere–mesosphere,  
404 respectively. Figure 8 shows spectra at three levels: 23, 27 and 31 km (lower, middle and upper panel,  
405 respectively).

406 It is seen that short periods <5 days are not statistically significant at these altitudes. Eastward  
407 wave 1 exhibit a maximum variance at 10–30 day periods (red curve in Fig. 8d–8f). Westward wave 1  
408 and eastward wave 2 (black and blue curves in Fig. 8d–8f) do not show clear periodicity peak and tend  
409 to be more intense at the longest periods, i.e. to be quasi-stationary. This is confirmed by spectra in  
410 Fig. 8g–8i. Westward wave 1 apparent from Fig. 8a–8c (black solid line along the wave ridge) is of  
411 highest spectral power in Fig. 8d–8f (black curve) and in Fig. 8g–8i (the black vertical line at wave  
412 number –1).

413 To examine the wave spectrum difference in the upper stratosphere–mesosphere before and after  
414 the SSW start that is suggested by Fig. 7, the two 40-day time intervals are compared in Fig. 9. These  
415 are 20 December–10 February and 10 February–31 March for the intervals of pre- and post SSW

416 initial date, respectively. It is seen from Fig. 9a–9e (Fig. 9f–9j) that eastward (westward) wave 1  
417 demonstrates maximum spectral signal before (after) the SSW start. Transition from eastward to  
418 westward propagated wave 1 is seen also from the wave number spectra in Fig. 9k–9o and Fig. 9p–9t),  
419 respectively. If the short and long periods (<5 days and >5 days) are present in the first interval, then  
420 the periods longer than 10 days dominate in the second interval (Fig. 9k–9o and Fig. 9p–9t,  
421 respectively).

422 The role of wave 1 and wave 2 in the SSW preconditioning and development is known from many  
423 studies (Matsuno, 1971; Charlton et al., 2007; Manney et al., 2009; Yuan et al., 2012; Limpasuvan et  
424 al., 2016; Rao et al., 2018). Our spectral analysis (Fig. 8 and Fig. 9) reveals the changes in the wave  
425 spectra associated with the SSW onset and their altitudinal dependence.

426  
427

## 428 **5 Discussion**

429

430 The observations of the major SSW effects in February 2018 in the NH midlatitude mesosphere by  
431 microwave radiometer at the Kharkiv site, Northern Ukraine (50.0°N, 36.3°E), have been provided.  
432 The CO altitude profiles in the mesosphere have been measured by the MWR with one-day time  
433 resolution. Using the CO molecule as a tracer, the wind speed has been retrieved from the Doppler  
434 shift of the CO 115.3 GHz emission and the mesospheric winds reverse from westerly to easterly  
435 below the winter mesopause region (70–85 km) has been detected. A few ground-based observations  
436 in the mesosphere by the same method have been undertaken at midlatitudes (Sect. 1). The zonal wind  
437 and CO profile variability during the major SSW were compared with the daily zonal wind,  
438 temperature, zonal wave 1/wave 2 and geopotential height datasets from the MLS data, the ERA-  
439 Interim, and MERRA-2 reanalyses. The SSW started with the polar vortex split around 10 February  
440 (Fig. 1), zonal wind reverse in the mesosphere and stratosphere (Fig. 2b and Fig. 5) and enhanced  
441 stratosphere warming and mesosphere cooling (Fig. 2a).

442 Among the most striking SSW manifestations over the midlatitude station in February 2018, there  
443 were (i) zonal wind reversal throughout the mesosphere–stratosphere, (ii) oscillations in the vertical  
444 profiles of CO, zonal wind and temperature, (iii) descent of the stratospheric CO and temperature  
445 anomalies on the time scale of days to months, (iv) change from the eastward to westward wave 1  
446 around the starting date of the SSW and (v) strong mesospheric CO and westerly peaks at the start of  
447 the SSW recovery phase. The midlatitude SSW effects are known from many event analyses and in  
448 most cases they are associated with zonal asymmetry and polar vortex split and displacements relative  
449 to the pole (Solomon et al., 1985; Allen et al., 1999; Yuan et al., 2012; Chandran and Collins, 2014).  
450 Our results show that the local midlatitude atmosphere variability in the SSW 2018 combines both the

451 large-scale changes in the zonal circulation and temperature typical for the SSWs and the altitude-  
452 dependent planetary wave patterns and their evolution in the individual vortex split event.

453

454

## 455 **5.1 Wave patterns and CO level**

456

457 As noted in Sect. 1, CO abundance in the extratropical mesosphere increases with latitude toward the  
458 winter pole due to meridional transport. CO accumulation results in the formation of the CO layer with  
459 the sharp vertical gradient at its lower edge (Solomon et al., 1985; Shepherd et al., 2014). The  
460 horizontal CO gradient at the polar vortex edge also exists and the vortex split and displacement of the  
461 pole associated with the SSW cause significant CO variability at the NH midlatitudes (Solomon et al.,  
462 1985; Allen et al., 1999; Funke et al., 2009; Shepherd et al., 2014).

463 In Sect. 4a, based on the MWR observations, we have defined the lower CO edge at 6 ppmv and  
464 this edge uplifted during the SSW by about 8 km (between 75 km and 83 km, thick part of the white  
465 curve in Fig. 3a). This uplifting noticeably stands out against the pre- and post-SSW variations of the  
466 6-ppmv level occurring within 2–3 km (Fig. 4a). The MLS CO measurements show similar variations  
467 in the 6-ppmv level over the Kharkiv region (white curve in Fig. 3b) and their absence in the  
468 corresponding zonal mean (yellow curve in Fig. 3a, 3b, and 3e).

469 Mesospheric CO profile uplifting is usually associated with the stratopause elevation during the  
470 SSW, when air, poor in CO, enters the mesospheric CO layer from below (Kvissel et al., 2012;  
471 Shepherd et al., 2014). Similar ascending motions in the stratopause and mesopause regions were  
472 observed in the 2013 SSW from nitric oxide (NO) and showed that the NO contours deflected upwards  
473 throughout the mesosphere (Orsolini et al., 2017). Our analysis reveals that the local CO profile  
474 variations during the SSW 2018 were closely associated with the changes in the planetary wave  
475 patterns in the mesosphere.

476 The MLS CO distribution demonstrates how deformation, elongation (wave 2 effect) and rotation  
477 of the CO-rich polar area influence the local CO level over Kharkiv (white circle with respect to the  
478 CO contours in Fig. 4a–4h and Fig. S1). The highest elevation of the 6-ppmv CO level in Fig. 3a and  
479 3b corresponds to the lowest CO level over Kharkiv on 19–23 February, when the most distant  
480 displacement of the CO contours 16 ppmv and 6 ppmv off the Kharkiv location was observed (Fig. 4c  
481 and 4g, respectively; see also the third column in Fig. S1). As known, the strong vertical CO gradient  
482 in the winter mesosphere is found at the higher altitudes in the tropics than in the extratropics  
483 (Solomon et al., 1985; Allen et al., 1999; Garcia et al., 2014). Then, poleward displacement of the low-  
484 latitude air masses is accompanied by the CO abundance decrease and vertical CO gradient elevation  
485 at the middle latitudes, as it is observed in Fig. 3a and 3b. A similar effect related to the wave 1

486 influence was observed during the 2003–2004 Arctic warming (Funke et al., 2009): the vortex has  
487 shifted from the pole toward the western sector and mid-latitude air poor in CO filled the eastern sector  
488 (0–90°E) over 50–80°N and even over the pole.

489 The results of Fig. 4 and Fig. S1 show that meridional displacements of the low-latitude, CO-poor  
490 mesospheric air to the Kharkiv region occurred under the planetary wave influence and caused the  
491 local CO profile variations in the SSW 2018 (Fig. 3a and 3b). These results, thus, confirm that  
492 latitudinal displacements due to wave effects may dramatically affect the local densities of the  
493 atmospheric species (Solomon et al., 1985). Figure 6a demonstrates that the local stratopause elevation  
494 in February 2018 to about 60 km was relatively small in comparison with the elevation that is  
495 characteristic for the polar region, up to 70–80 km (Chandran et al., 2011; Tomikawa et al., 2012;  
496 Limpasuvan et al., 2016; Orsolini et al., 2010, 2017). No significant stratopause elevation was  
497 observed in the zonal mean for 47.5–52.5°N (Fig. 6b). Therefore, the meridional (poleward) and zonal  
498 displacements of the CO-rich air masses enclosed within the polar vortex (Solomon et al., 1985; Allen  
499 et al., 1999; Funke et al., 2009) rather than stratopause elevation (Kvissel et al., 2012; Shepherd et al.,  
500 2014) may be dominant cause of the CO profile uplift observed in the NH midlatitudes during the  
501 SSW 2018.

502 In March 2018, after the SSW, vertical CO profile has been re-established (Fig. 3a and 3b)  
503 according to the recovery phase following the SSW (Shepherd et al., 2014; Limpasuvan et al., 2016).  
504 In the MWR data, the SSW recovery phase in the mesosphere in early March started with the short-  
505 term but anomalously high peaks in the local CO (Fig. 3a) and westerly wind (Fig. 5a). These peaks  
506 reached the highest values in daily variations of CO and zonal wind over the three months of the  
507 observations (January–March). By analogy with the low-CO episode in February discussed above, the  
508 high-CO peak in early March 2018 caused by change in the vortex shape and return of the CO-rich  
509 vortex edge region to the Kharkiv location (compare 2–6 March in Fig. 4d and 4h with 19–23 February  
510 in Fig. 4c and 4g; see also the same dates in Fig. S2).

511 Wind measurements using the CO layer provides a further means to evaluate the validity of the  
512 modeled winds. Furthermore, by combining the measurements with ray tracing of gravity wave  
513 propagation (e.g. Kogure et al., 2018), this type of measurement may provide particular insights into  
514 wave-mean flow interactions, particularly where local temperature inversions alter gravity wave  
515 filtering (Hocke et al., 2018; Fritts et al., 2018).

516  
517  
518  
519  
520

## 521 **5.2 Descent of the midlatitude stratospheric anomalies**

522

523 Alternating altitudinal sequence of warm and cool anomalies progressively descended through the  
524 mesosphere and stratosphere of the polar region was observed in January–March 2018 (Fig. 2a) in  
525 consistency with many observations (Zhou et al., 2002; Orsolini et al., 2010; Shepherd et al., 2014; de  
526 Wit et al., 2014; Zülicke et al., 2018). The warm anomaly sharply intensified in the stratosphere  
527 between 20 and 50 km with simultaneous strong cooling in the mesosphere in the active phase of SSW  
528 since 10 February (vertical arrow in Fig. 2a). Unlike this, the midlatitude temperature anomalies do not  
529 show the similar vertical arrangement and regular descent with respect to the same mean climatology  
530 2005–2017 (Fig. S4).

531 During the SSW of 2018, the upper (lower) stratosphere over the Kharkiv region was cooler  
532 (warmer) up to 20°C (10°C) than climatological mean with stepwise descent relative to the pre-SSW  
533 one (Fig. S4a). However, excluding unstable anomalies at different altitudes, the air temperature  
534 through the mesosphere and stratosphere was close to the climatology during most of the time in  
535 January–March 2018 (light blue in Fig. S4a). The zonal mean temperature anomalies show steady  
536 warming of the air in the stratosphere and lower mesosphere and distinct tendency for the anomaly to  
537 descend between about 40 km and 20 km during the SSW (20 days,  $\sim -1 \text{ km}\cdot\text{day}^{-1}$ ). It could be  
538 concluded that the temperature anomaly profile observed in the NH midlatitudes may vary in time  
539 depending on the observing location and individual SSW event and, thus, differ from climatologically  
540 warm (cold) stratospheric (mesospheric) anomaly typical for the SSWs in the NH polar region (e.g.  
541 Chandran and Collins, 2014; their Fig. 1g).

542 The CO profiles in Fig. 3 demonstrate opposite tendencies in the vertical shift of the CO-rich air in  
543 the NH midlatitudes. The CO descent in the stratosphere occurred during January–February with  
544 velocities of about 270 and 220  $\text{m}\cdot\text{day}^{-1}$  in a case of the regional and zonal mean data, respectively  
545 (Fig. 3d and 3g). In general, this is in a range of the winter descent velocities observed in the polar  
546 vortex (Funke et al., 2009; Salmi et al., 2011; Ryan et al., 2018), however, a few times lower than in  
547 the polar vortex in the winter 2017–2018 (Fig. 2a). The deepest penetration of the mesospheric CO  
548 levels (0.1–0.5 ppmv) to  $\sim 30$  km was observed immediately after the SSW onset (Fig. 3d and 3g).  
549 Although this coincides with the peaks in the wave 1 and wave 2 amplitudes (Fig. 2e), the main reason  
550 in the CO increase in the stratosphere over Kharkiv is the location of the small sub-vortex of the  
551 splitted polar vortex (9–13 February, Fig. 4n).

552 The MLS CO maps in Fig. 4 show that the high CO amount is concentrated inside the polar vortex  
553 and its fragments after splitting. This is a result of meridional and downward transport of CO that is  
554 strongest in the winter polar vortex (Rinsland et al., 1999; Manney et al., 2009; Kvissel et al., 2012;



555 Shepherd et al., 2014). Before (4–8 February), during (19–23 February) and after (2–6 March) the  
556 SSW, Kharkiv was outside the stratospheric vortex/sub-vortices edge (Fig. 4m, 4o and 4p,  
557 respectively) and the CO amount was at low level typical for the midlatitude stratosphere (of about  
558 0.01–0.02 ppmv; Engel et al., 2006; Huret et al., 2006; Funke et al. 2009). Descent of the 0.1-ppmv  
559 contour marked by dashed lines in Fig. 3d and 3g is observed due to the episodic shift of the vortex  
560 edge toward the Kharkiv region or to the corresponding zone 47.5–52.5°N, respectively.

561 Figure 4 demonstrates that the CO amount inside the polar vortex or its fragments is much higher  
562 than in the surrounding area not only in the mesosphere but also in the stratosphere. This leads to the  
563 possibility of the enhanced CO appearance even in the stratosphere at about 25–30 km (Engel et al.,  
564 2006; Huret et al., 2006; Funke et al., 2009). By analogy, the vortex edge shift beyond the Kharkiv  
565 region (Fig 4c and 4g) resulted in lowering of the regional CO mixing ratios in the mesosphere  
566 consistent to both ground-based and satellite observations (Fig. 3a and 3b, respectively). Meridional  
567 structure of the mesospheric CO (Sect. 1) provided the uplift of the 6-ppmv level during the SSW  
568 relative to pre- and post-SSW levels (Fig. 3a and 3b).

569

570

### 571 **5.3 Wave spectrum changes**

572

573 As known, amplified wave 1 and wave 2 are dominant zonal wave numbers in the stratosphere and  
574 mesosphere that precede the SSW and cause zonal wind reversal and polar vortex displacement off the  
575 pole (wave 1) or vortex split (wave 2) at the start and during the SSW (Matsuno, 1971; Charlton et al.,  
576 2007; Manney et al., 2009; Yuan et al., 2012; Limpasuvan et al., 2016). Variations in the wave  
577 amplitudes (Fig. 2e) are a possible cause of the oscillations in CO, zonal wind and temperature  
578 described in Sect. 4. In addition to variability in the anomaly intensity, the character of the zonal  
579 circulation is under the wave influence on the different SSW phase (Sect. 4.2). Particularly, the  
580 spectral composition of the waves is reflected in the temperature anomaly zonal migration (Sect. 4.4)  
581 to which less attention was given in the earlier studies. Clear change from eastward to westward  
582 anomaly propagation is seen in the upper stratosphere–mesosphere at the SSW initial date, 10  
583 February 2018 (Fig. 7 and Fig. S3) and it coincides with the zonal wind reversal from westerly to  
584 easterly (Fig. 2b and Fig. 5). Corresponding changes occurred in the wave spectra (Fig. 9) with  
585 prevailing eastward (westward) wave 1 before (after) 10 February.

586 The simulations made by Limpasuvan et al. (2016) show that the westward propagating planetary  
587 wave 1 forcing dominates above 70 km in the winter hemisphere with the SSW onset. Since upward  
588 planetary wave propagation is limited in the easterly zonal flow (Charney and Drazin, 1961), the  
589 presence of in situ forced planetary waves around the SSW onset due to the jet instability in the

590 underlying polar mesosphere is discussed (Limpasuvan et al., 2016, and references herein).  
591 Limpasuvan et al. (2016) have shown that spectral power of the westward wave 1 increases around the  
592 SSW onset also in the 40–60 km layer (their Fig. 10b) and this effect may be caused by unstable  
593 westward polar jet below 80 km. The results of Section 4.4 (Fig. 9) suggest that some kind of  
594 instability and westward wave forcing down to the upper stratosphere is possible in the midlatitudes.  
595 This possibility needs to be examined in the simulations.

596  
597

## 598 **6 Conclusions**

599

600 The impact of a major sudden stratospheric warming (SSW) in February 2018 on the mid-latitude  
601 mesosphere was investigated using microwave radiometer measurements in Kharkiv, Ukraine (50.0°N,  
602 36.3°E). The zonal wind reversal has been revealed below the winter mesopause region at 70–85 km  
603 altitudes during the SSW using the CO profiles. The reverse of the mesospheric westerly from about  
604  $10 \text{ m s}^{-1}$  to easterly wind about  $-10 \text{ m s}^{-1}$  around 10 February has been documented. The data from the  
605 ERA-Interim and MERRA-2 reanalyses and the Aura MLS temperature profiles have been used for the  
606 analysis of stratosphere–mesosphere behavior under the SSW conditions. Our local microwave  
607 observations in the NH midlatitude combined with the reanalysis data show wide ranges of daily  
608 variability in CO, zonal wind and temperature in the mesosphere and stratosphere during the SSW  
609 2018.

610 Among the most striking SSW manifestations over the midlatitude station in February 2018, there  
611 were (i) zonal wind reversal throughout the mesosphere–stratosphere, (ii) oscillations in the vertical  
612 profiles of CO, zonal wind and temperature, (iii) descent of the stratospheric CO and temperature  
613 anomalies on the time scale of days to months, (iv) wave 2 peak at the vortex split date and change  
614 from the eastward to westward wave 1 during the SSW and (v) strong mesospheric CO and westerly  
615 peaks at the start of the SSW recovery phase. Generally, the midlatitude SSW effects are known from  
616 many event analyses and in most cases they are associated with zonal asymmetry and polar vortex split  
617 and displacements relative to the pole (Solomon et al., 1985; Allen et al., 1999; Yuan et al., 2012;  
618 Chandran and Collins, 2014). From our results, the local midlatitude atmosphere variability in the  
619 SSW 2018 combine both the large-scale changes in the zonal circulation and temperature typical for  
620 the SSWs and local evolution of the altitude-dependent planetary wave patterns in the individual  
621 vortex split event.

622 The observed local CO variability can be explained mainly by horizontal air mass redistribution  
623 due to planetary wave activity with the replacement of the CO-rich air by CO-poor air and vice versa,  
624 in agreement with other studies. The MLS CO fields show that the CO-rich air masses are enclosed

625 within the polar vortex. Horizontal (meridional and zonal) displacements of the edge of the vortex or  
626 vortex fragments relative to the ground-based midlatitude station may be a dominant cause of the  
627 observed CO profile variations during the SSW 2018. The small sub-vortex located over the station at  
628 the SSW start caused the appearance of the enhanced CO level not only in the mesosphere but also in  
629 the stratosphere at about 30 km. This indicates that the polar vortex contains the CO-rich air masses  
630 with much higher CO amount than in the surrounding area and this takes place over the stratosphere–  
631 mesosphere altitude range.

632 Microwave observations show that sharp altitudinal CO gradient below the mesopause could be  
633 used to define the lower edge of the CO layer and to evaluate oscillation and significant elevation of  
634 the lower CO edge during the SSW and its trend on a seasonal time scale. The presented results of  
635 microwave measurements of CO and zonal wind in the midlatitude mesosphere at 70–85 km altitudes,  
636 which is still not adequately covered by ground-based observations (Hagen et al., 2018; Rüfenacht et  
637 al., 2018), are suitable for evaluating and potentially improving atmospheric models. Simulations show  
638 that planetary wave forcing by westward propagating wave 1 dominates between 40 and 80 km in the  
639 winter polar region during the SSW (Limpasuvan et al., 2016). Our spectral analysis reveals that the  
640 westward wave 1 during the SSW 2018 is a dominant wave component through the midlatitude upper  
641 stratosphere–mesosphere. Instability of the westward polar jet suggested in previous studies (e.g.  
642 Limpasuvan et al., 2016) should be analyzed in the context of the westward wave 1 generation in the  
643 midlatitude upper stratosphere–mesosphere.

644 Our observation of variability of the CO layer during the SSW deserves further study, particularly  
645 in relation to the implications for modelling of wave dynamics and vertical coupling (Ern et al., 2016;  
646 Martineau et al., 2018) and chemical processes (Garcia et al., 2014) in the mesosphere.

647

648

649 *Conflict of Interest.* The authors declare that the research was conducted in the absence of any  
650 commercial or financial relationships that could be construed as a potential conflict of interest.

651

652 *Author contributions.* GM coordinated and led the efforts for this manuscript. VS initiated the  
653 microwave measurements during the SSW event in Kharkiv. VS, DS, VM and AA developed  
654 equipment and provided microwave measurements with data processing by AP and DS. GM, VS, YW,  
655 OE, AK, and AG analyzed the results and provided interpretation. GM, OE, AK, VS, and WH wrote  
656 the paper with input from all authors.

657

658

659 *Acknowledgments.* This work was supported in part by the Institute of Radio Astronomy of the  
660 National Academy of Sciences of Ukraine; by Taras Shevchenko National University of Kyiv, project  
661 19BF051-08; by the College of Physics, International Center of Future Science, Jilin University,  
662 China. The microwave radiometer data have been processed using ARTS and Qpack software  
663 packages (<http://www.radiativetransfer.org/>). Daily datasets from ERA-Interim reanalysis of European  
664 Centre for Medium-Range Weather Forecast (ECMWF) were downloaded from  
665 <https://www.ecmwf.int/en/forecasts/datasets/archive-datasets/reanalysis-datasets/era-interim>. The Aura  
666 Microwave Limb Sounder (MLS) measurements of air temperature and CO were obtained from  
667 <https://mls.jpl.nasa.gov/data/readers.php>. Zonal waves were analyzed using the National Oceanic and  
668 Atmospheric Administration National Centers for Environmental Prediction, Global Data Assimilation  
669 System–Climate Prediction Center (NOAA NCEP GDAS–CPC) data at  
670 <https://www.cpc.ncep.noaa.gov/products/stratosphere/strat-trop/> and the MERRA-2 data from the  
671 National Aeronautics and Space Administration Goddard Space Flight Center, Atmospheric Chemistry  
672 and Dynamics Laboratory (NASA GFC ACDL) site at [https://acd-](https://acd-ext.gsfc.nasa.gov/Data_services/met/ann_data.html)  
673 [ext.gsfc.nasa.gov/Data\\_services/met/ann\\_data.html](https://acd-ext.gsfc.nasa.gov/Data_services/met/ann_data.html). Authors thank the two anonymous reviewers for  
674 their valuable comments and useful suggestions.

675

676

## 677 **References**

678

- 679 Alexander, S. P. and Shepherd, M. G.: Planetary wave activity in the polar lower stratosphere, *Atmos.*  
680 *Chem. Phys.*, 10, 707–718, <https://doi.org/10.5194/acp-10-707-2010>, 2010.
- 681 Allen, D. R., Stanford, J. L., López-Valverde, M. A., Nakamura, N., Lary, D. J., Douglass, A. R.,  
682 Cerniglia, M. C., Remedios, J. J., and Taylor F. W.: Observations of middle atmosphere CO from  
683 the UARS ISAMS during the early northern winter 1991/92, *J. Atmos. Sci.*, 56, 563–583, 1999.
- 684 Baldwin, M. P. and Dunkerton, T. J.: Stratospheric harbingers of anomalous weather regimes, *Science*,  
685 294, 581–584, doi:10.1126/science.1063315, 2001.
- 686 Buehler, S. A., Mendrok, J., Eriksson, P., Perrin, A., Larsson, R., and Lemke, O.: ARTS, the  
687 atmospheric radiative transfer simulator – version 2.2, the planetary toolbox edition, *Geosci. Model*  
688 *Dev.*, 11, 1537–1556, doi:10.5194/gmd-11-1537-2018, 2018.
- 689 Butler, A. H. and Gerber, E. P. Optimizing the definition of a sudden stratospheric warming,  
690 *J. Climate*, 31, 2337–2344, doi:10.1175/JCLI-D-17-0648.1, 2018.
- 691 Butler, A. H., Seidel, D. J., Hardiman, S. C., Butchart, N., Birner, T., and Match, A.: Defining sudden  
692 stratospheric warmings, *Bull. Amer. Meteor. Soc.*, 96, 1913–1928, doi:10.1175/bams-d-13-  
693 00173.1, 2015.

694 Butler, A. H., Sjöberg, J. P., Seidel, D. J., and Rosenlof, K. H.: A sudden stratospheric warming  
695 compendium, *Earth Syst. Sci. Data*, 9, 63–76, doi:10.5194/essd-9-63-2017, 2017.

696 Chandran, A. and Collins, R. L.: Stratospheric sudden warming effects on winds and temperature in  
697 the middle atmosphere at middle and low latitudes: a study using WACCM, *Ann. Geophys.*, 32,  
698 859–874, doi:10.5194/angeo-32-859-2014, 2014.

699 Chandran, A., Collins, R. L., Garcia, R. R., and Marsh, D. R.: A case study of an elevated stratopause  
700 generated in the Whole Atmosphere Community Climate Model, *Geophys. Res. Lett.*, 38, L08804,  
701 doi:10.1029/2010GL046566, 2011.

702 [Charlton, A. J. and Polvani, L. M.: A new look at stratospheric sudden warmings. Part I: Climatology  
703 and modeling benchmarks. \*J. Climate\*, 20, 449–469, 2007.](#)

704 [Charney, J. G. and Drazin, P. G.: Propagation of planetary-scale disturbances from the lower into the  
705 upper atmosphere, \*J. Geophys. Res.\*, 66, 83–109, doi:10.1029/JZ066i001p00083, 1961.](#)

706 Dee, D. P., Uppala, S. M., Simmons, A. J., Berrisford, P., Poli, P., Kobayashi, S., Andrae, U.,  
707 Balmaseda, M. A., Balsamo, G., Bauer, P., Bechtold, P., Beljaars, A. C. M., van de Berg, L.,  
708 Bidlot, J., Bormann, N., Delsol, C., Dragani, R., Fuentes, M., Geer, A. J., Haimberger, L., Healy,  
709 S. B., Hersbach, H., Hólm, E. V., Isaksen, I., Kållberg, P., Köhler, M., Matricardi, M., McNally,  
710 A. P., Monge-Sanz, B. M., Morcrette, J.-J., Park, B. K., Peubey, C., de Rosnay, P., Tavolato, C.,  
711 Thépaut, J.-N., and Vitart, F.: The ERA-Interim reanalysis: configuration and performance of the  
712 data assimilation system, *Q. J. Roy. Meteor. Soc.*, 137, 553–597, doi:10.1002/qj.828, 2011.

713 de la Torre, L., Garcia, R. R., Barriopedro, D., and Chandran, A.: Climatology and characteristics of  
714 stratospheric sudden warmings in the Whole Atmosphere Community Climate Model, *J. Geophys.*  
715 *Res.*, 117, D04110, doi:10.1029/2011JD016840, 2012.

716 de Wit, R. J., Hibbins, R. E., Espy, P. J., Orsolini, Y. J., Limpasuvan, V., and Kinnison, D. E.:  
717 Observations of gravity wave forcing of the mesopause region during the January 2013 major  
718 Sudden Stratospheric Warming, *Geophys. Res. Lett.*, 41, 4745–4752, doi:10.1002/2014GL060501,  
719 2014.

720 Di Biagio, C., Muscari, G., di Sarra, A., de Zafra, R. L., Eriksen, P., Fiocco, G., Fiorucci, I., and Fuà,  
721 D.: Evolution of temperature, O<sub>3</sub>, CO, and N<sub>2</sub>O profiles during the exceptional 2009 Arctic major  
722 stratospheric warming as observed by lidar and millimeter wave spectroscopy at Thule (76.5N,  
723 68.8W), Greenland, *J. Geophys. Res.*, 115, D24315, doi:10.1029/2010JD014070, 2010.

724 [Engel, A., Möbius, T., Haase, H.-P., Bönisch, H., Wetter, T., Schmidt, U., Levin, I., Reddman, T.,  
725 Oelhaf, H., Wetzell, G., Grunow, K., Huret, N., and Pirre, M.: Observation of mesospheric air  
726 inside the arctic stratospheric polar vortex in early 2003, \*Atmos. Chem. Phys.\*, 6, 267–282,  
727 doi:10.5194/acp-6-267-2006, 2006.](#)

728 Eriksson, P., Buehler, S. A., Davis, C. P., Emde, C., and Lemke, O.: ARTS, the atmospheric radiative  
729 transfer simulator, version 2, *J. Quant. Spectrosc. Radiat. Transfer*, 112, 1551–1558, doi:  
730 10.1016/j.jqsrt.2011.03.001, 2011.

731 Eriksson, P., Jiménez, C., and Buehler, S. A.: Qpack, a tool for instrument simulation and retrieval  
732 work, *J. Quant. Spectrosc. Radiat. Transfer*, 91, 47–64, doi: 10.1016/j.jqsrt.2004.05.050, 2005.

733 Ern, M., Trinh, Q. T., Kaufmann, M., Krisch, I., Preusse, P., Ungermann, J., Zhu, Y., Gille, J. C.,  
734 Mlynczak, M. G., Russell III, J. M., Schwartz, M. J., and Riese, M.: Satellite observations of  
735 middle atmosphere gravity wave absolute momentum flux and of its vertical gradient during recent  
736 stratospheric warmings, *Atmos. Chem. Phys.*, 16, 9983–10019, [https://doi.org/10.5194/acp-16-](https://doi.org/10.5194/acp-16-9983-2016)  
737 9983-2016, 2016.

738 Feng, W., Kaifler, B., Marsh, D. R., Höffner, J., Hoppe, U.-P., Williams, B. P., and Plane J. M. C.:  
739 Impacts of a sudden stratospheric warming on the mesospheric metal layers, *J. Atmos. Solar-Terr.*  
740 *Phys.*, 162, 162–171, 2017.

741 Forkman, P., Christensen, O. M., Eriksson, P., Urban, J., and Funke, B.: Six years of mesospheric CO  
742 estimated from ground-based frequency-switched microwave radiometry at 57° N compared with  
743 satellite instruments, *Atmos. Meas. Tech.*, 5, 2827–2841, doi: 10.5194/amt-5-2827-2012, 2012.

744 Forkman, P., Christensen, O. M., Eriksson, P., Billade, B., Vassilev, V., and Shulga, V. M.: A compact  
745 receiver system for simultaneous measurements of mesospheric CO and O<sub>3</sub>, *Geosci. Instrum.*  
746 *Method. Data Syst.*, 5, 27–44, doi:10.5194/gi-5-27-2016, 2016.

747 Fritts, D. C., Laughman, B., Wang, L., Lund, T. S., and Collins, R. L.: Gravity wave dynamics in a  
748 mesospheric inversion layer: 1. Reflection, trapping, and instability dynamics. *J. Geophys. Res.-*  
749 *Atmos.*, 123, 626–648, <https://doi.org/10.1002/2017JD027440>, 2018.

750 Funke, B., López-Puertas, M., García-Comas, M., Stiller, G. P., von Clarmann, T., Höpfner, M.,  
751 Glatthor, N., Grabowski, U., Kellmann, S., and Linden, A.: Carbon monoxide distributions from  
752 the upper troposphere to the mesosphere inferred from 4.7μm non-local thermal equilibrium  
753 emissions measured by MIPAS on Envisat, *Atmos. Chem. Phys.*, 9, 2387–2411,  
754 <https://doi.org/10.5194/acp-9-2387-2009>, 2009.

755 Garcia, R. R., López-Puertas, M., Funke, B., Marsh, D. R., Kinnison, D. E., Smith, A. K., and  
756 González-Galindo, F.: On the distribution of CO<sub>2</sub> and CO in the mesosphere and lower  
757 thermosphere, *J. Geophys. Res.-Atmos.*, 119, 5700–5718, doi:10.1002/2013JD021208, 2014.

758 Gardner, C. S.: Role of wave induced diffusion and energy flux in the vertical transport of atmospheric  
759 constituents in the mesopause region, *J. Geophys. Res.-Atmos.*, 123, 6581–6604,  
760 <https://doi.org/10.1029/2018JD028359>, 2018.

761 Goldsmith, P. F., Litvak, M. M., Plambeck, R. L., and Williams, D. R.: Carbon monoxide mixing  
762 ratios in the mesosphere derived from ground-based microwave measurements, *J. Geophys. Res.*,  
763 84, 416–418, 1979.

764 Hagen, J., Murk, A., Rüfenacht, R., Khaykin, S., Hauchecorne, A., and Kämpfer, N.: WIRA-C: a  
765 compact 142-GHz-radiometer for continuous middle-atmospheric wind measurements. *Atmos.*  
766 *Meas. Tech.*, 11, 5007–5024, doi: 10.5194/amt-11-5007-2018, 2018.

767 Hocke, K., Lainer, M., Bernet, L., and Kämpfer, N.: Mesospheric inversion layers at mid-latitudes and  
768 coincident changes of ozone, water vapour and horizontal wind in the Middle Atmosphere.  
769 *Atmosphere*, 9, 171, <https://doi.org/10.3390/atmos9050171>, 2018.

770 Hoffmann, C. G., Raffalski, U., Palm, M., Funke, B., Golchert, S. H. W., Hochschild, G., and Notholt,  
771 J.: Observation of strato-mesospheric CO above Kiruna with ground-based microwave radiometry  
772 – retrieval and satellite comparison, *Atmos. Meas. Tech.*, 4, 2389–2408,  
773 <https://doi.org/10.5194/amt-4-2389-2011>, 2011.

774 [Hu, J., Ren, R., and Xu, H.: Occurrence of winter stratospheric sudden warming events and the  
775 seasonal timing of spring stratospheric final warming, \*J. Atmos. Sci.\*, 71, 2319–2334,  
776 doi:10.1175/JAS-D-13-0349.1, 2014.](#)

777 [Huret, N., Pirre, M., Hauchecorne, A., Robert, C., and Catoire V.: On the vertical structure of the  
778 stratosphere at midlatitudes during the first stage of the polar vortex formation and in the polar  
779 region in the presence of a large mesospheric descent, \*J. Geophys. Res.\*, 111, D06111,  
780 doi:10.1029/2005JD006102, 2006.](#)

781 Karpechko, A. Yu., Charlton-Perez, A., Balmaseda, M., Tyrrell, N., and Vitart, F.: Predicting sudden  
782 stratospheric warming 2018 and its climate impacts with a multimodel ensemble, *Geophys. Res.*  
783 *Lett.*, 24, 13538–13546, <https://doi.org/10.1029/2018GL081091>, 2018.

784 Keuer, D., Hoffmann, P., Singer, W., and Bremer, J.: Long-term variations of the mesospheric wind  
785 field at mid-latitudes, *Ann. Geophys.*, 25, 1779–1790, doi:10.5194/angeo-25-1779-2007, 2007.

786 Kogure, M., Nakamura, T., Ejiri, M. K., Nishiyama, T., Tomikawa, Y., and Tsutsumi, M.: Effects of  
787 horizontal wind structure on a gravity wave event in the middle atmosphere over Syowa (69°S,  
788 40°E), the Antarctic, *Geophys. Res. Lett.*, 45, 5151–5157. <https://doi.org/10.1029/2018GL078264>,  
789 2018.

790 Koo, J.-H., Walker, K. A., Jones, A., Sheese, P. E., Boone, C. D., Bernath, P. F., and Manney, G. L.:  
791 Global climatology based on the ACE-FTS version 3.5 dataset: Addition of mesospheric levels and  
792 carbon-containing species in the UTLS, *J. Quant. Spectrosc. Radiat. Transfer*, 186, 52–62,  
793 doi:10.1016/j.jqsrt.2016.07.003, 2017.

794 Kuttippurath, J. and Nikulin, G.: A comparative study of the major sudden stratospheric warmings in  
795 the Arctic winters 2003/2004–2009/2010, *Atmos. Chem. Phys.*, 12, 8115–8129,  
796 <https://doi.org/10.5194/acp-12-8115-2012>, 2012.

797 Kvissel, O. K., Orsolini, Y. J., Stordal, F., Limpasuvan, V., Richter, J., and Marsh, D. R.: Mesospheric  
798 intrusion and anomalous chemistry during and after a major stratospheric sudden warming. *J.*  
799 *Atmos. Solar-Terr. Phys.*, 78–79, 116–124, doi:10.1016/j.jastp.2011.08.015, 2012.

800 Limpasuvan, V., Orsolini, Y. J., Chandran, A., Garcia, R. R., and Smith, A. K.: On the composite  
801 response of the MLT to major sudden stratospheric warming events with elevated stratopause, *J.*  
802 *Geophys. Res.-Atmos.*, 121, 4518–4537, doi:10.1002/2015JD024401, 2016.

803 Manney, G. L., Schwartz, M. J., Krüger, K., Santee, M. L., Pawson, S., Lee, J. N., Daffer, W. H.,  
804 Fuller, R. A., and Livesey, N. J.: Aura Microwave Limb Sounder observations of dynamics and  
805 transport during the record-breaking 2009 Arctic stratospheric major warming, *Geophys. Res.*  
806 *Let.*, 36, L12815, doi:10.1029/2009GL038586, 2009.

807 Martineau, P., Son, S.-W., Taguchi, M., and Butler, A. H.: A comparison of the momentum budget in  
808 reanalysis datasets during sudden stratospheric warming events, *Atmos. Chem. Phys.*, 18, 7169–  
809 7187, <https://doi.org/10.5194/acp-18-7169-2018>, 2018.

810 Matsuno, T.: A dynamical model of the stratospheric sudden warming, *J. Atmos. Sci.*, 28, 1479–1494,  
811 [https://doi.org/10.1175/1520-0469\(1971\)028<1479:ADMOTS>2.0.CO;2](https://doi.org/10.1175/1520-0469(1971)028<1479:ADMOTS>2.0.CO;2), 1971.

812 Muscari, G., di Sarra, A., de Zafra, R. L., Lucci, F., Baordo, F., Angelini, F., and Fiocco, G.: Middle  
813 atmospheric O<sub>3</sub>, CO, N<sub>2</sub>O, HNO<sub>3</sub>, and temperature profiles during the warm Arctic winter 2001–  
814 2002, *J. Geophys. Res.*, 112, D14304, doi:10.1029/2006JD007849, 2007.

815 Newnham, D. A., Ford, G. P., Moffat-Griffin, T., and Pumphrey, H. C.: Simulation study for  
816 measurement of horizontal wind profiles in the polar stratosphere and mesosphere using ground-  
817 based observations of ozone and carbon monoxide lines in the 230–250 GHz region, *Atmos. Meas.*  
818 *Tech.*, 9, 3309–3323, doi:10.5194/amt-9-3309-2016, 2016.

819 Orsolini, Y. J., Limpasuvan, V., Pérot, K., Espy, P., Hibbins, R., Lossow, S., Larsson, K. R., and  
820 Murtagh, D.: Modelling the descent of nitric oxide during the elevated stratopause event of January  
821 2013, *J. Atmos. Solar-Terr. Phys.*, 155, 50–61, doi:10.1016/j.jastp.2017.01.006, 2017.

822 Orsolini, Y. J., Urban, J., Murtagh, D. P., Lossow, S., and Limpasuvan, V.: Descent from the polar  
823 mesosphere and anomalously high stratopause observed in 8 years of water vapor and temperature  
824 satellite observations by the Odin Sub-Millimeter Radiometer, *J. Geophys. Res.*, 115, D12305,  
825 doi:10.1029/2009JD013501, 2010.

826 Pedatella, N. M., Chau, J. L., Schmidt, H., Goncharenko, L. P., Stolle, C., Hocke, K., Harvey, V. L.,  
827 Funke, B., and Siddiqui, T. A.: How sudden stratospheric warming affects the whole atmosphere,  
828 *Eos*, 99, available at <https://doi.org/10.1029/2018EO092441>, 2018.



- 829 Piddyachiy, V., Shulga, V., Myshenko, V., Korolev, A., Antyufeyev, O., Shulga, D., and Forkman, P.:  
830 Microwave radiometer for spectral observations of mesospheric carbon monoxide at 115 GHz over  
831 Kharkiv, Ukraine, *J. Infrared Milli. Terahz. Waves*, 38, 292–302, doi:10.1007/s10762-016-0334-1,  
832 2017.
- 833 Piddyachiy, V. I., Shulga, V. M., Myshenko, V. V., Korolev, A. M., Myshenko, A. V., Antyufeyev, A.  
834 V., Poladich, A. V., and Shkodin, V. I.: 3-mm wave spectroradiometer for studies of atmospheric  
835 trace gases. *Radiophys Quantum El.*, 53(5-6), 326–333. [https://doi.org/10.1007/s11141-010-](https://doi.org/10.1007/s11141-010-9231-y)  
836 [9231-y](https://doi.org/10.1007/s11141-010-9231-y), 2010.
- 837 [Rao, J., Ren, R.-C., Chen, H., Liu, X., Yu, Y., and Yang, Y.: Sub-seasonal to seasonal hindcasts of](#)  
838 [stratospheric sudden warming by BCC\\_CSM1.1\(m\): A comparison with ECMWF. \*Adv. Atmos.\*](#)  
839 [Sci., 36, 479–494, doi:10.1007/s00376-018-8165-8, 2019.](#)
- 840 Rao, J., Ren, R., Chen, H., Yu, Yu., and Zhou, Y.: The stratospheric sudden warming event in  
841 February 2018 and its prediction by a climate system model, *J. Geophys. Res.-Atmos.*, 123,  
842 13332–13345, doi:10.1029/2018JD028908, 2018.
- 843 Rinsland, C. P., Salawitch, R. J., Gunson, M. R., Solomon, S., Zander, R., Mahieu, E., Goldman, A.,  
844 Newchurch, M. J., Irion, F. W., and Chang, A. Y.: Polar stratospheric descent of NO<sub>y</sub> and CO and  
845 Arctic denitrification during winter 1992–1993, *J. Geophys. Res.*, 104, 1847–1861, 1999.
- 846 Rüfenacht, R., Baumgarten, G., Hildebrand, J., Schranz, F., Matthias, V., Stober, G., Lübken, F.-J.,  
847 and Kämpfer, N.: Intercomparison of middle-atmospheric wind in observations and models,  
848 *Atmos. Meas. Tech.*, 11, 1971–1987, <https://doi.org/10.5194/amt-11-1971-2018>, 2018.
- 849 [Rüfenacht, R., Hocke, K., and Kämpfer, N.: First continuous ground-based observations of long period](#)  
850 [oscillations in the vertically resolved wind field of the stratosphere and mesosphere, \*Atmos. Chem.\*](#)  
851 [Phys., 16, 4915-4925, https://doi.org/10.5194/acp-16-4915-2016, 2016.](#)
- 852 Rüfenacht, R., Kämpfer, N., and Murk, A.: First middle-atmospheric zonal wind profile measurements  
853 with a new ground-based microwave Doppler-spectroradiometer, *Atmos. Meas. Tech.*, 5, 2647–  
854 2659, doi:10.5194/amt-5-2647-2012, 2012.
- 855 [Ryan, N. J. Kinnison, D. E., Garcia, R. R., Hoffmann, C. G., Palm, M., Raffalski, U., and Notholt, J.:](#)  
856 [Assessing the ability to derive rates of polar middle-atmospheric descent using trace gas](#)  
857 [measurements from remote sensors, \*Atmos. Chem. Phys.\*, 18, 1457–1474,](#)  
858 <https://doi.org/10.5194/acp-18-1457-2018>, 2018.
- 859 Ryan, N. J., Palm, M., Raffalski, U., Larsson, R., Manney, G., Millán, L., and Notholt, J.: Strato-  
860 mesospheric carbon monoxide profiles above Kiruna, Sweden (67.8°N, 20.4°E), since 2008, *Earth*  
861 *Syst. Sci. Data*, 9, 77–89, doi:10.5194/essd-9-77-2017, 2017.
- 862 Salmi, S. M., Verronen, P. T., Thölix, L., Kyrölä, E., Backman, L., Karpechko, A. Yu., and Seppälä,  
863 A.: Mesosphere-to-stratosphere descent of odd nitrogen in February–March 2009 after sudden

864 stratospheric warming, *Atmos. Chem. Phys.*, 11, 4645–4655, [https://doi.org/10.5194/acp-11-4645-](https://doi.org/10.5194/acp-11-4645-2011)  
865 2011, 2011.

866 Scheiben, D., Straub, C., Hocke, K., Forkman, P., and Kämpfer, N.: Observations of middle  
867 atmospheric H<sub>2</sub>O and O<sub>3</sub> during the 2010 major sudden stratospheric warming by a network of  
868 microwave radiometers, *Atmos. Chem. Phys.*, 12, 7753–7765, [https://doi.org/10.5194/acp-12-](https://doi.org/10.5194/acp-12-7753-2012)  
869 7753-2012, 2012.

870 Shepherd, M. G., Beagley, S. R., and Fomichev, V. I.: Stratospheric warming influence on the  
871 mesosphere/lower thermosphere as seen by the extended CMAM, *Ann. Geophys.*, 32, 589–608,  
872 [doi:10.5194/angeo-32-589-2014](https://doi.org/10.5194/angeo-32-589-2014), 2014.

873 Solomon, S., Garcia, R. R., Olivero, J. J., Bevilacqua, R. M., Schwartz, P. R., Clancy, R. T., and  
874 Muhleman, D. O.: Photochemistry and transport of carbon monoxide in the middle atmosphere, *J.*  
875 *Atmos. Sci.*, 42, 1072–1083, 1985.

876 Stray, N. H., Orsolini, Y. J., Espy, P. J., Limpasuvan, V., and Hibbins, R. E.: Observations of planetary  
877 waves in the mesosphere-lower thermosphere during stratospheric warming events, *Atmos. Chem.*  
878 *Phys.*, 15, 4997–5005, <https://doi.org/10.5194/acp-15-4997-2015>, 2015.

879 Tao, M., Konopka, P., Ploeger, F., Groöß, J.-U., Müller, R., Volk, C. M., Walker, K. A., and Riese,  
880 M.: Impact of the 2009 major sudden stratospheric warming on the composition of the  
881 stratosphere, *Atmos. Chem. Phys.*, 15, 8695–8715, <https://doi.org/10.5194/acp-15-8695-2015>,  
882 2015.

883 Taguchi, M.: Comparison of subseasonal-to-seasonal model forecasts for major stratospheric sudden  
884 warmings, *J. Geophys. Res.-Atmos.*, 123, 10,231–10,247, [doi:10.1029/2018jd028755](https://doi.org/10.1029/2018jd028755), 2018.

885 Tomikawa, Y., Sato, K., Watanabe, S., Kawatani, Y., Miyazaki, K., and Takahashi, M.: Growth of  
886 planetary waves and the formation of an elevated stratopause after a major stratospheric sudden  
887 warming in a T213L256 GCM, *J. Geophys. Res.*, 117, D16101, [doi:10.1029/2011JD017243](https://doi.org/10.1029/2011JD017243), 2012.

888 Tripathi, O. P., Baldwin, M., Charlton-Perez, A., Charron, M., Cheung, J. C. H., Eckermann, S. D.,  
889 Gerber, E., Jackson, D. R., Kuroda, Yu., Lang, A., McLay, J., Mizuta, R., Reynolds, C., Roff, G.,  
890 Sigmond, M., Son, S.-W., and Stockdale, T.: Examining the predictability of the stratospheric  
891 sudden warming of January 2013 Using Multiple NWP Systems, *Mon. Weather Rev.*, 144, 1935–  
892 1960, [doi:10.1175/mwr-d-15-0010.1](https://doi.org/10.1175/mwr-d-15-0010.1), 2016.

893 Vargin, P. N. and Kiryushov, B. M.: Major sudden stratospheric warming in the Arctic in February  
894 2018 and its impacts on the troposphere, mesosphere, and ozone layer, *Russian Meteorology and*  
895 *Hydrology*, 44, 112–123, [doi:10.3103/S1068373919020043](https://doi.org/10.3103/S1068373919020043), 2019.

896 Waters, J. W., Wilson, W. J., and Shimabukuro, F. I.: Microwave measurement of mesospheric carbon  
897 monoxide, *Science*, 191, 1174–1175, [doi:10.1126/science.191.4232.1174](https://doi.org/10.1126/science.191.4232.1174), 1976.

898 WMO Commission for Atmospheric Sciences. Abridged Final Report of the Seventh Session, Manila,  
899 27 February – 10 March, 1978. WMO-No. 509, 113 p., available at:  
900 [http://library.wmo.int/pmb\\_ged/wmo\\_509\\_en.pdf](http://library.wmo.int/pmb_ged/wmo_509_en.pdf), 1978.

901 Xu, X., Manson, A. H., Meek, C. E., Chshyolkova, T., Drummond, J. R., Hall, C. M., Riggin, D. M.,  
902 and Hibbins, R. E.: Vertical and interhemispheric links in the stratosphere-mesosphere as revealed  
903 by the day-to-day variability of Aura-MLS temperature data, *Ann. Geophys.*, 27, 3387–3409,  
904 doi:10.5194/angeo-27-3387-2009, 2009.

905 Yu, Y., Cai, M., Shi, C., and Ren, R.: On the linkage among strong stratospheric mass circulation,  
906 stratospheric sudden warming, and cold weather events, *Mon. Weather Rev.*, 146, 2717–2739,  
907 doi:10.1175/MWR-D-18-0110.1, 2018.

908 Yuan, T., Thuraiajah, B., She, C. Y., Chandran, A., Collins, R. L., and Krueger, D. A.: Wind and  
909 temperature response of midlatitude mesopause region to the 2009 Sudden Stratospheric Warming,  
910 *J. Geophys. Res.*, 117, D09114, doi:10.1029/2011JD017142, 2012.

911 Zhou, S., Miller, A. J., Wang, J., and James, K. A.: Downward-propagating temperature anomalies in  
912 the preconditioned polar stratosphere, *J. Climate*, 15, 781–792, doi:10.1175/1520-  
913 0442(2002)015<0781:DPTAIT>2.0.CO;2, 2002.

914 Zülicke, C. and Becker, E.: The structure of the mesosphere during sudden stratospheric warmings in a  
915 global circulation model, *J. Geophys. Res.-Atmos.*, 118, 2255–2271, doi:10.1002/jgrd.50219,  
916 2013.

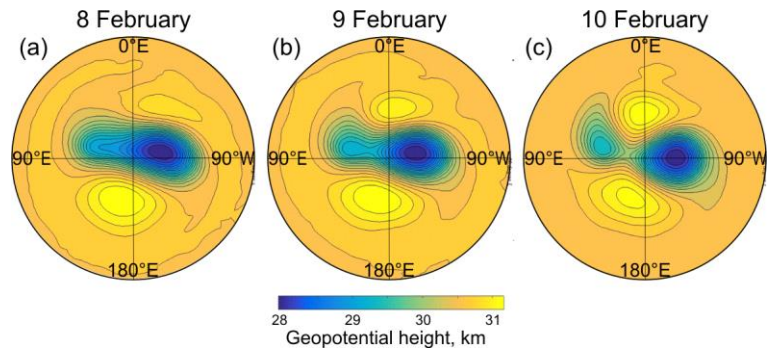
917 Zülicke, C., Becker, E., Matthias, V., Peters, D. H. W., Schmidt, H., Liu, H.-L., de la Torre Ramos, L.,  
918 and Mitchell, D. M.: Coupling of stratospheric warmings with mesospheric coolings in  
919 observations and simulations, *J. Climate*, 31, 1107–1133, doi:10.1175/JCLI-D-17-0047, 1, 2018.

920

921

922

923



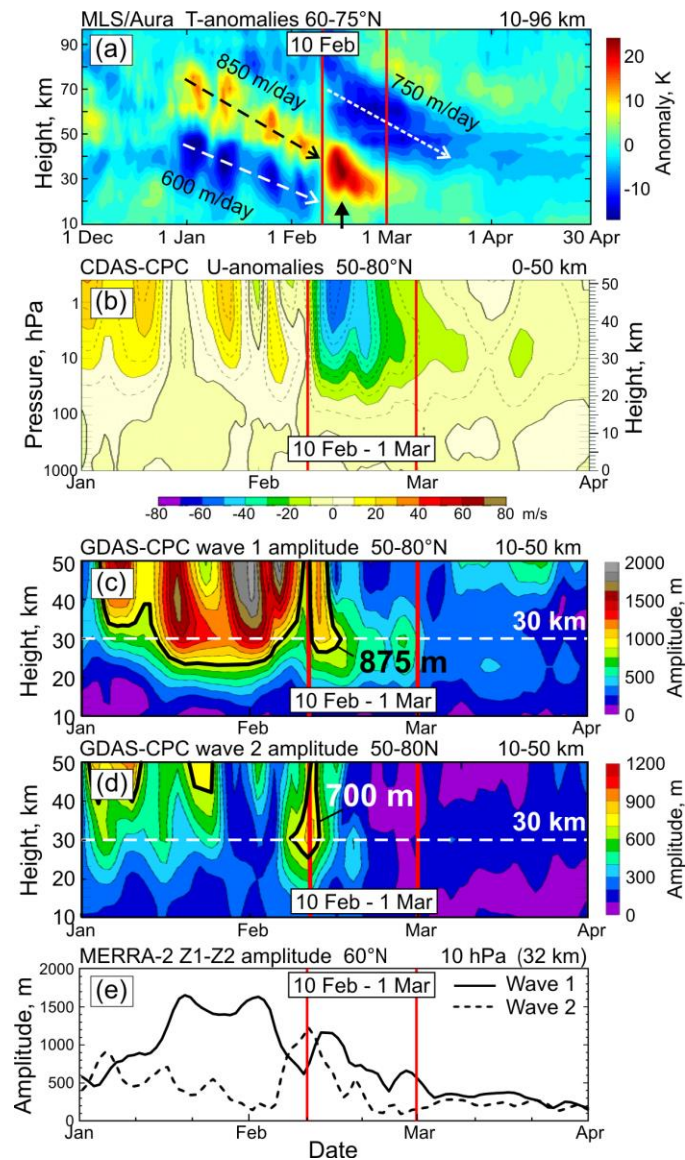
924

925

926 **Figure 1.** The polar vortex split at the 10-hPa pressure level during the SSW event in February 2018.

927 Geopotential heights are calculated from ERA-Interim reanalysis data.

928



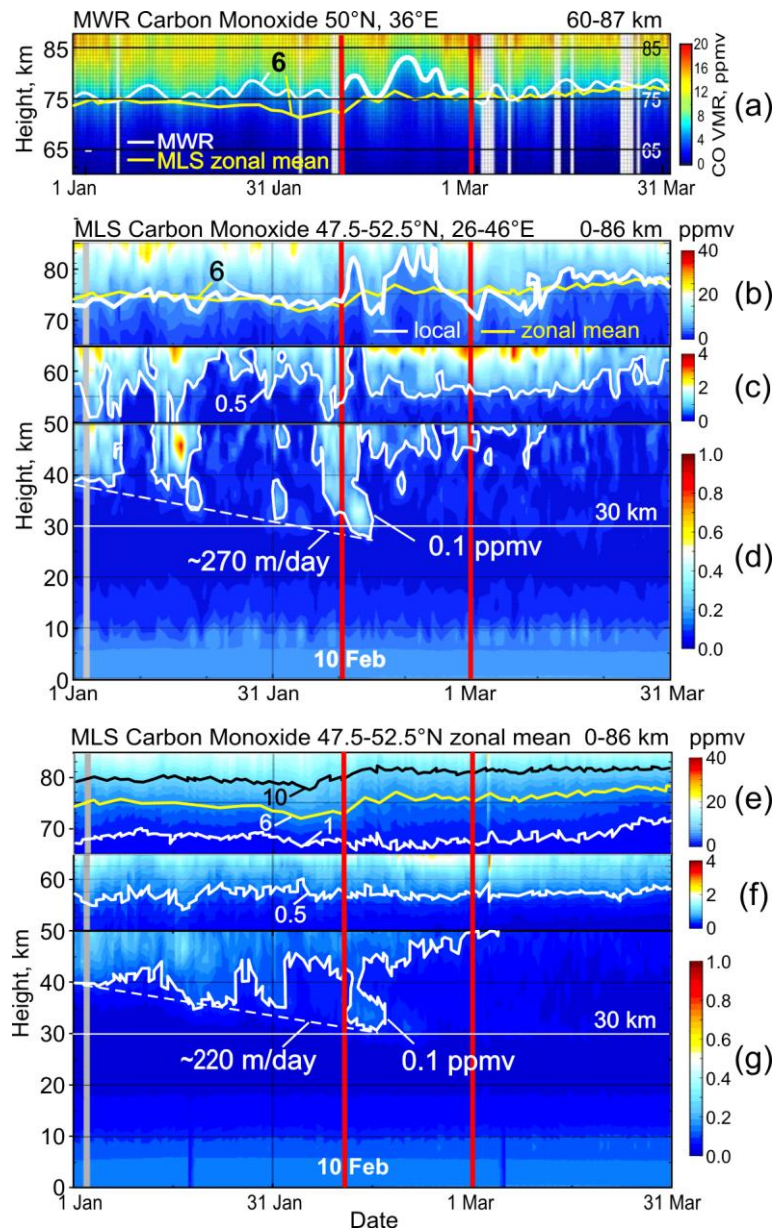
930

931

932 **Figure 2.** The development of the SSW in 2018 from the vertical profiles of (a) Aura MLS  
 933 temperature anomalies in December 2017–April 2018 at polar zone 60–75°N (with respect to the mean  
 934 climatology 2005–2017), (b) zonal mean zonal wind anomalies, (c) wave 1 and (d) wave 2 amplitudes  
 935 in geopotential height in January–March by NOAA NCEP GDAS-CPC data (climatology 1981–2010).  
 936 (e) zonal wave 1 and wave 2 amplitudes in geopotential height at 10 hPa, 60°N, by the MERRA-2 time  
 937 series from the NASA GFC ACDL data. The SSW-related anomalous variability between 10 February  
 938 and 1 March 2018 is bounded by red vertical lines.

939

940



942

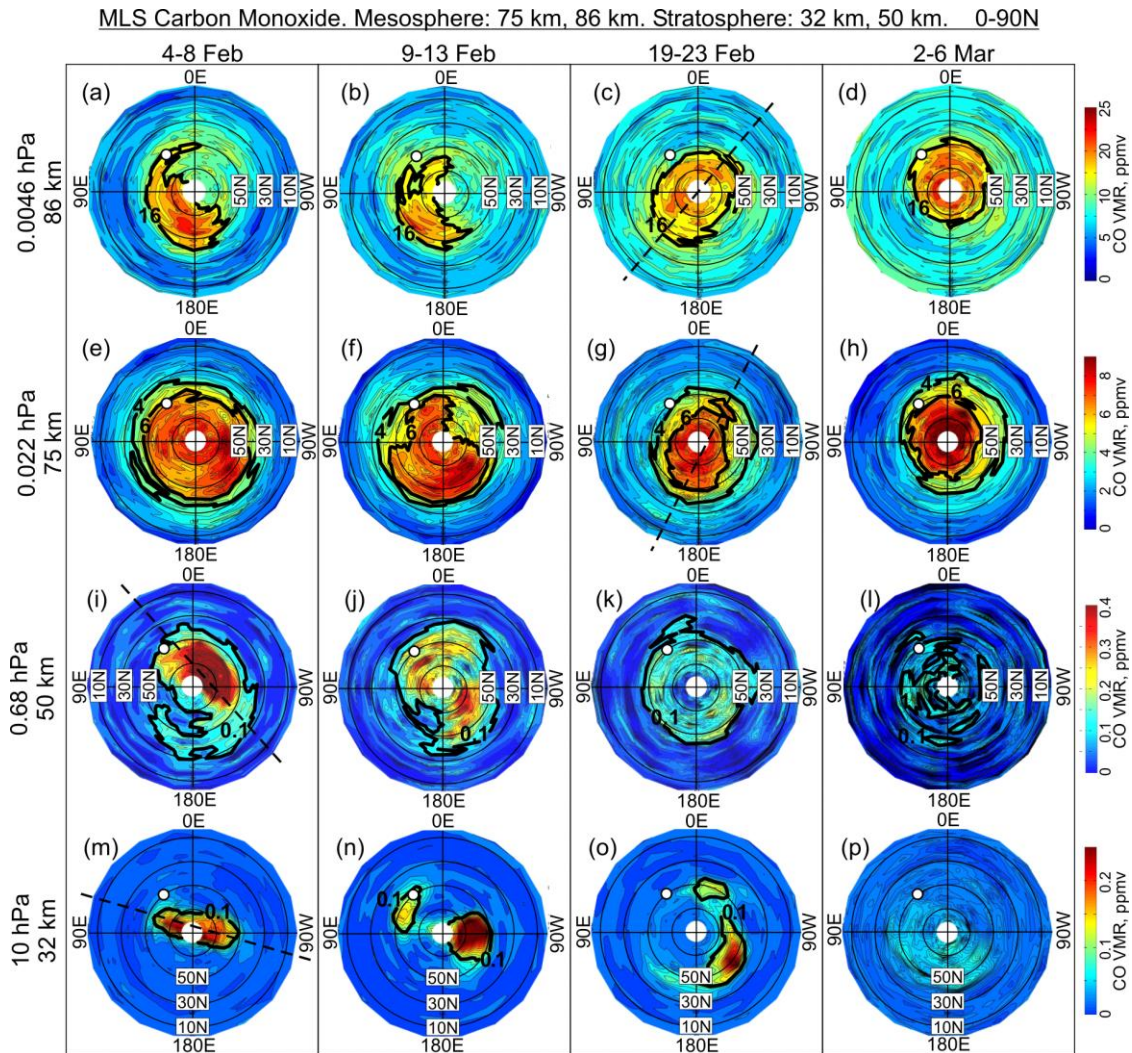
943

944 **Figure 3.** (a) Mesospheric CO profile from microwave measurements over Kharkiv averaged in  
 945 altitude range 70–85 km, and vertical CO profile from the MLS measurements averaged over latitudes  
 946 47.5–52.5°N and longitudes (b)–(d) 26–46°E centered at the Kharkiv MWR site (50°N, 36°E) and (e)–  
 947 (g) 0–360°E for zonal mean. Selected CO levels are highlighted by white, black and yellow contours  
 948 (see text for details). Data for January–March 2018 are presented and time interval of significant  
 949 variations in the atmosphere parameters due to the SSW event (from 10 February to 1 March 2018) is  
 950 bounded by red vertical lines.

951

952

953  
954  
955

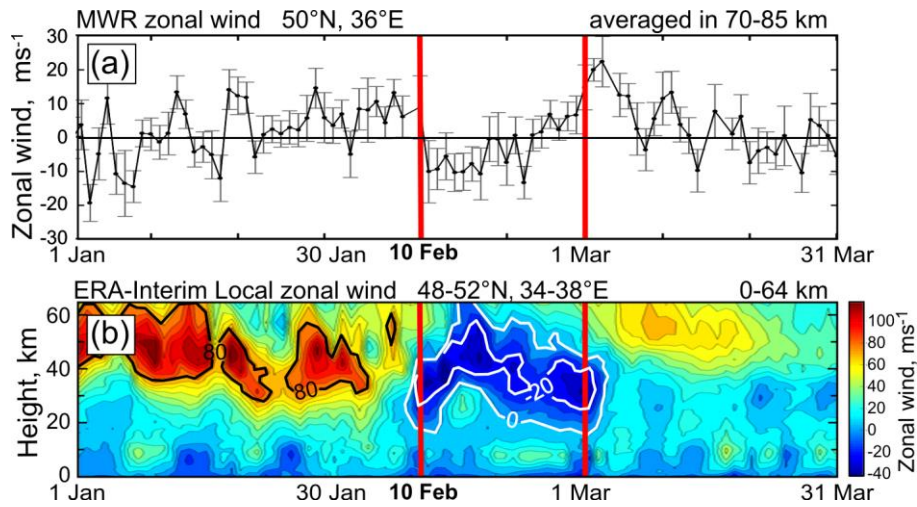


956  
957

958 **Figure 4.** The 5-day mean CO field over the NH (0–90°N) from the MLS measurements at the two  
959 mesospheric (75 km and 86 km) and stratospheric (32 km and 50 km) levels before (4–8 February),  
960 during (9–13 and 19–23 February) and after (2–6 March) the SSW 2018. White circle shows location  
961 of the MWR site Kharkiv relatively the high/low CO amounts marked off by the blue contours.  
962 Dashed lines indicate clockwise rotation of the elongated polar vortex with altitude as manifestation of  
963 upward propagation of planetary waves with their westward tilt with altitude.

964  
965  
966

967  
968  
969



970  
971

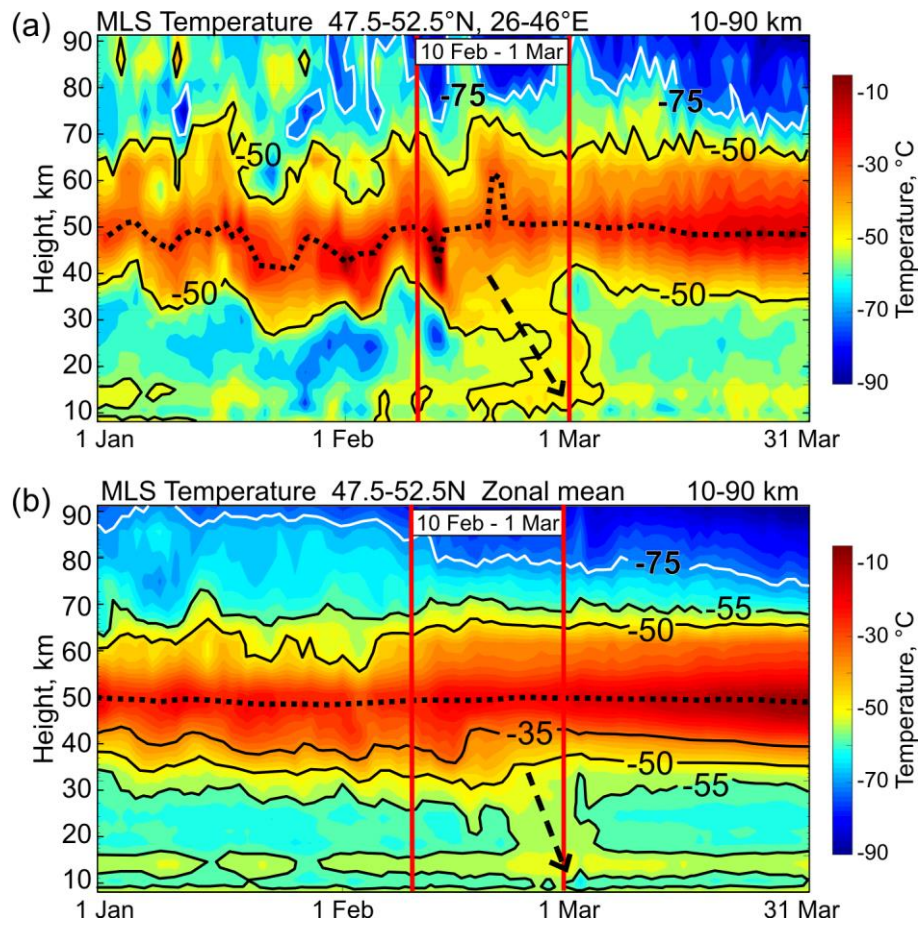
972 **Figure 5.** (a) Mesospheric zonal wind microwave measurements over Kharkiv (averaged in altitude  
973 range 70–85 km, vertical bars are standard deviations) compared to (b) time-altitude local zonal wind  
974 from the ERA-Interim reanalysis data averaged over latitudes 48–52°N and longitudes 34–38°E  
975 (centered at the Kharkiv microwave radiometer site, 50°N, 36°E ). Time interval of significant  
976 variations in the atmosphere parameters due to the SSW event (from 10 February to 1 March, 2018) is  
977 bounded by red vertical lines.

978  
979  
980



981

982



983

984

985 **Figure 6.** MLS temperature profiles (a) over the Kharkiv region and (b) zonal average in the zone  
986 47.5–52.5°N. Dashed arrows indicate downward warming.

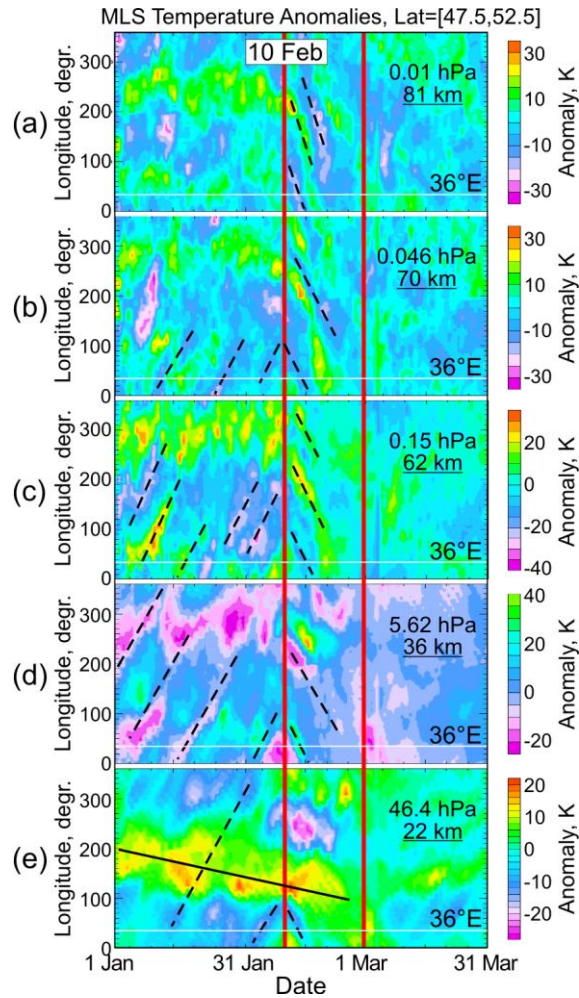
987

988

989

990

991



992

993

994 **Figure 7.** Time–longitude variations of the MLS temperature anomalies in the Kharkiv zone 47.5–  
995 52.5°N with respect to the mean climatology 2005–2017 during January–March 2018. Dashed lines  
996 show change of the zonal anomaly propagation from eastward to westward near 10 February, at the  
997 start of the SSW 2018.

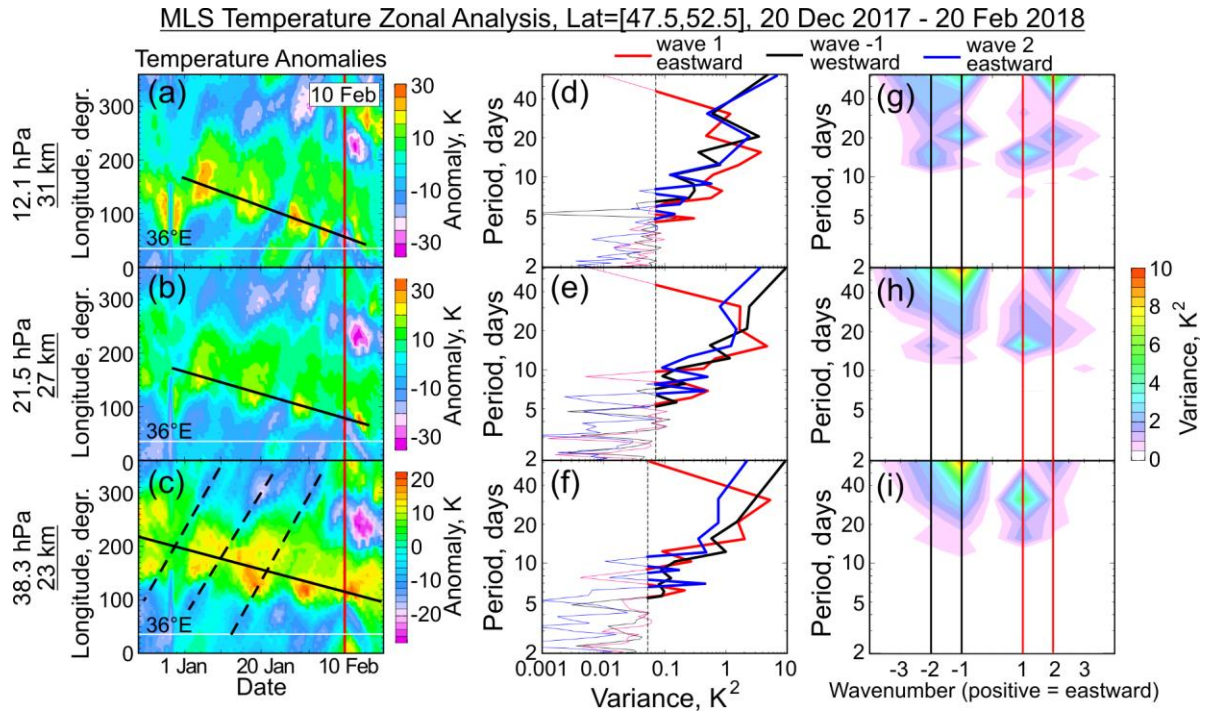
998

999

1000

1001

1002



1003

1004

1005

1006

1007

1008

1009

1010

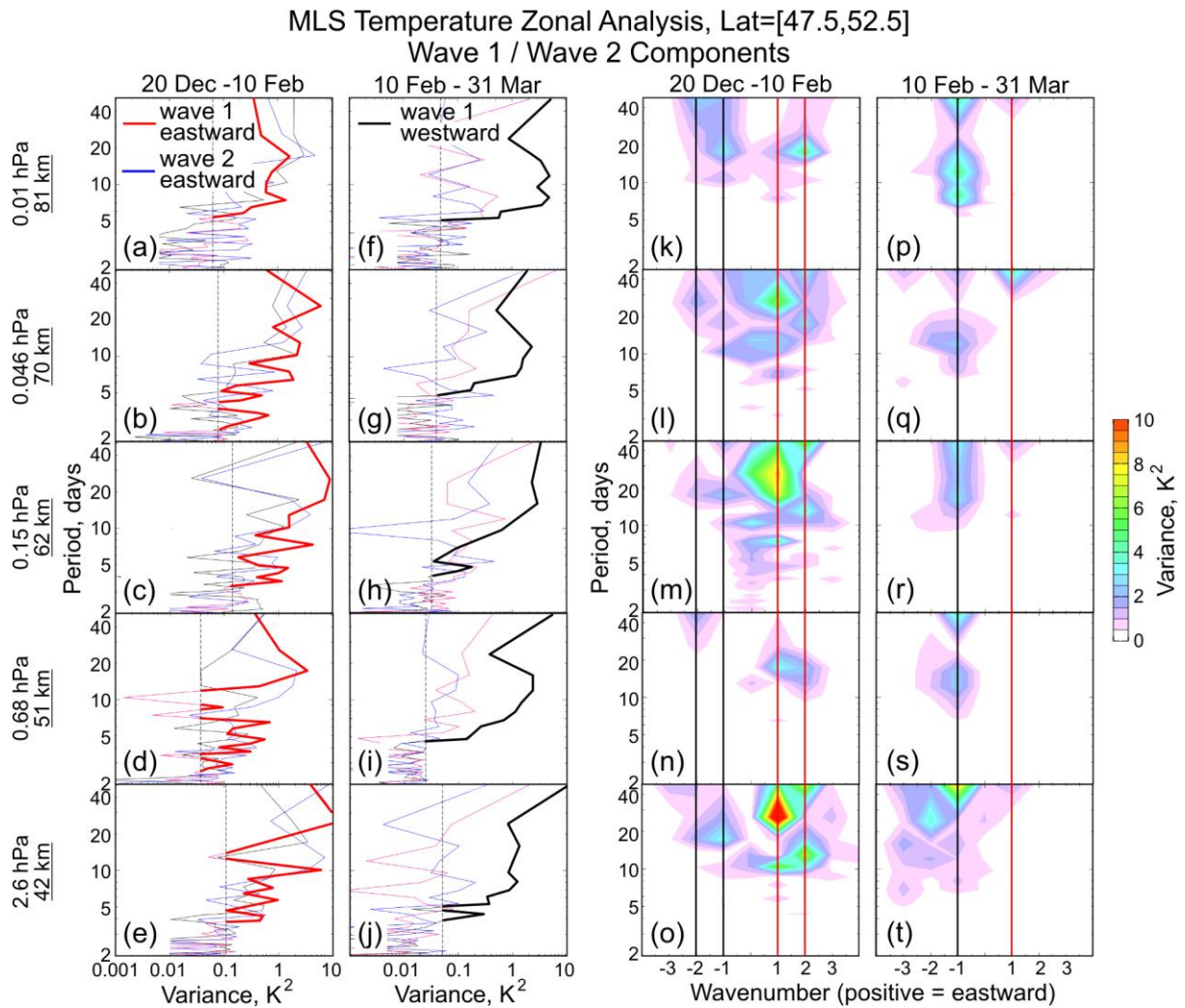
1011

1012

**Figure 8.** (left) As in Fig. 7, but for the zonal temperature anomalies in the lower–middle stratosphere at 23, 27 and 31 km (lower, middle and upper panels, respectively) during 20 December 2017 – 20 February 2018; (middle) wave 1 and wave 2 periods versus variance and (right) wave number spectra for the corresponding altitudes. Dashed line in the middle column marks the 95% confidence limit and bold curves highlight the wavenumber variance exceeding this limit.

1013

1014



1015

1016

1017 **Figure 9.** The spectral analysis of the zonal temperature anomalies as in Fig. 8 (middle and right) but  
 1018 for the upper stratosphere–mesosphere: (a–e, k–o) before and (f–j, p–t) after the SSW start on 10  
 1019 February 2018. Red and black lines indicate the eastward and westward propagating wavenumbers,  
 1020 respectively. Bold curves to the right of dashed line in (a–j) and spectra in (k–t) show the wavenumber  
 1021 variance exceeding the 95% confidence limit.

1022

1023

## Supplementary Material

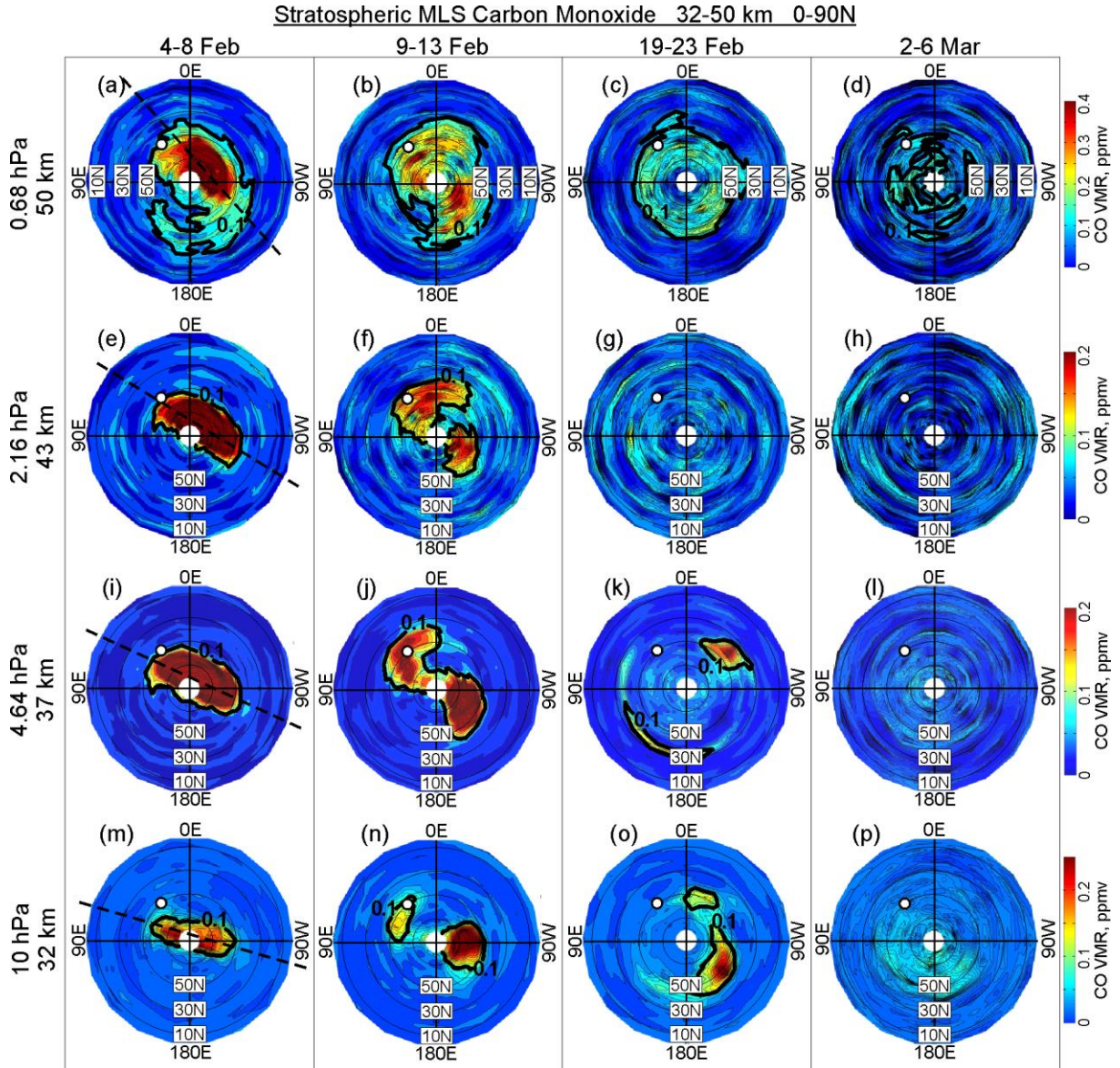
### Winter 2018 major sudden stratospheric warming impact on midlatitude mesosphere from microwave radiometer measurements, by Wang et al.

#### The description of the data used for analysis

The Aura MLS CO values have been taken from version 4.2x Aura MLS Level 2 data (<https://mls.jpl.nasa.gov/data/readers.php>). Aura MLS v4.2x data have 37 pressure levels. The useful range of CO data is from 215 hPa to 0.0046 hPa with corresponding height is from ~11 km to ~86 km. The satellite observation data points are divided into 20° longitude × 2° latitude grids. That means: longitude is divided into 180:20:180 and latitude is divided into 90:2:90 segments. Then the average value of the data is taken in the grid as the value of the center of the grid. For instance, the average in the grid of 180°–160° in longitude and 90°–88° in latitude is taken as the average value of 170° degrees in longitude and 89° in latitude.

Data are removed (replaced by ‘NaN’) if they do not meet the quality criteria described in ‘Version 4.2x Level 2 data quality and description document’ ([https://mls.jpl.nasa.gov/data/v4-2\\_data\\_quality\\_document.pdf](https://mls.jpl.nasa.gov/data/v4-2_data_quality_document.pdf)). The five-day average (Fig. S1 and S2) is not simply a sum, divided by five. If the data of a certain area is blank, the data of that area will be ignored on that day. For example, if the data of a certain area in five days are: A, B, NaN, C, NaN, the average value of this area is  $(A+B+C)/3$ .

Daily datasets from ERA-Interim global atmospheric reanalysis of European Centre for Medium-Range Weather Forecast have been used for comparison with microwave radiometer observations (<https://www.ecmwf.int/en/forecasts/datasets/archive-datasets/reanalysis-datasets/era-interim>). Two types of level in the ERA-Interim database were used: ‘Model level’ and ‘Pressure level’. The number vertical levels in ‘Model level’ and ‘Pressure level’ datasets are 60 and 37, respectively. The pressure ranges in ‘Model level’ and ‘Pressure level’ datasets are from the surface up to 0.1 hPa and 1 hPa, respectively. Horizontal dimension resolution (longitude×latitude) is selected as 0.75°×0.75°. The ‘Model type’ data are used for drawing temperature and zonal wind velocity profiles from surface up to 0.1 hPa in order to compare with the data measured by microwave radiometer in Kharkiv, which extends up to 87 km altitude. The ‘Pressure level’ data were used to create geopotential height plots (Fig.1).

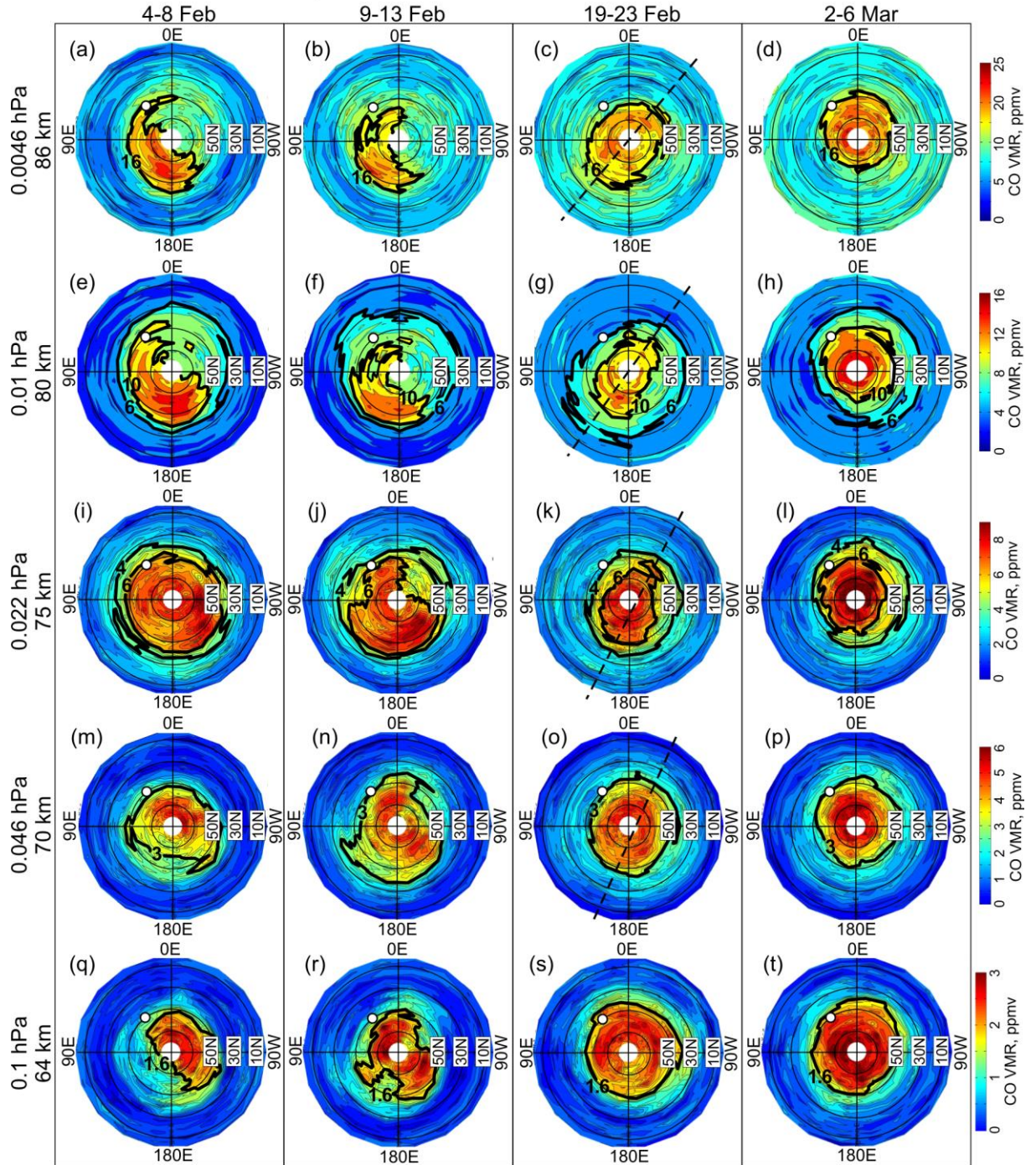


34

35 **Figure S1.** The 5-day mean CO fields in the NH stratosphere (0–90°N, between 32 km and 50  
 36 km) from the MLS measurements before (first column, 4–8 February), during (second and third  
 37 columns, 9–13 and 19–23 February, respectively) and after (forth column, 2–6 March) the SSW  
 38 2018. White circle shows location of the MWR site Kharkiv relatively the high/low CO  
 39 amounts marked off by the black contours. Note that Kharkiv falls under the area of high CO  
 40 amount just after the SSW start (second column, 9–13 February) due to the westward rotation  
 41 of the polar air mass caused by the zonal wind reverse from westerly to easterly. The high CO  
 42 anomalies disappear after the SSW (right column, 2–6 March). Dashed lines indicate planetary  
 43 wave westward tilt with altitude.

44

Mesospheric MLS Carbon Monoxide 64-86 km 0-90N



45

46 **Figure S2.** As in Fig. S1, but for the NH mesosphere (0–90°N, between 64 km and 86 km).

47 Note that the lowest mesospheric CO levels observed with the MWR in February 2018 over

48 Kharkiv (white curve for 6 ppmv in Fig. 3a) are explained by the westward displacement of the

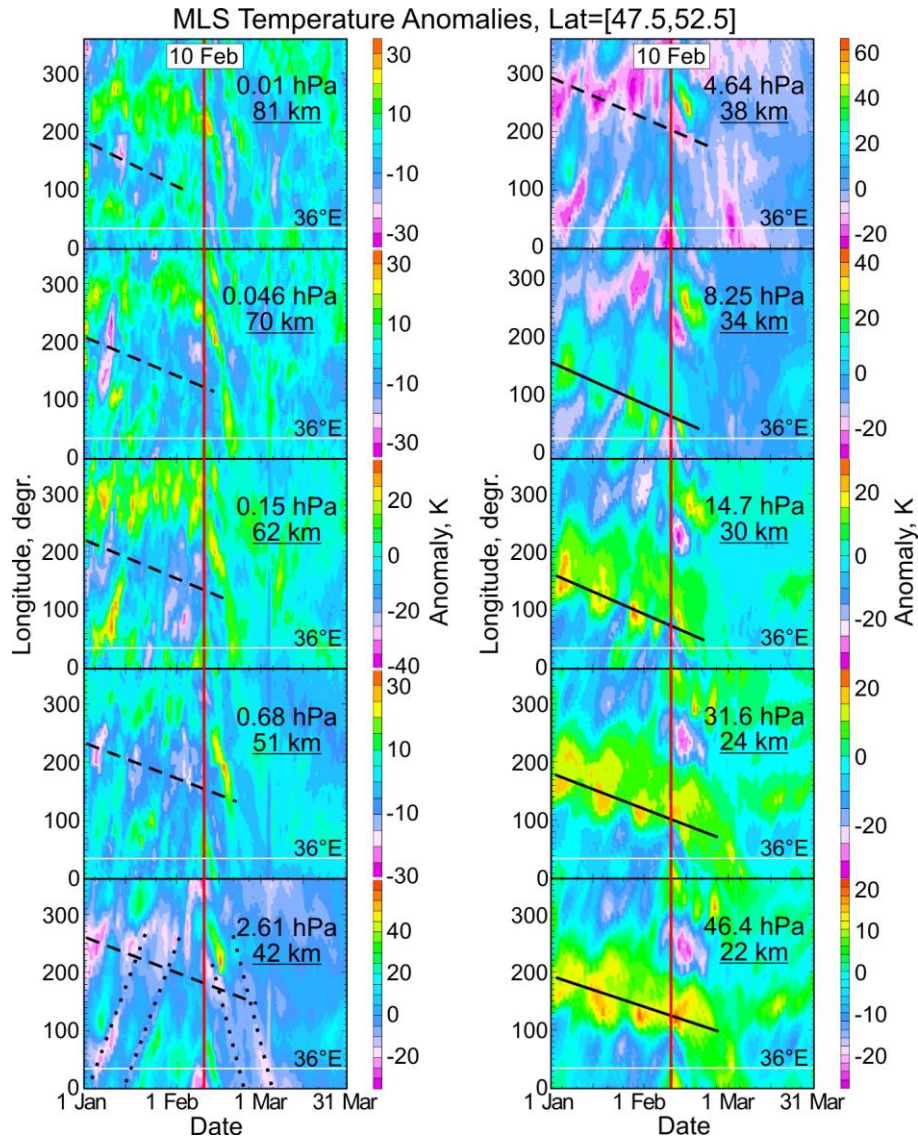
49 boundary between the low- and high-CO polar air mass (compare the Kharkiv location relative

50 to the contour 16 ppmv in (a–c), 6 ppmv in (e–g) and 4 ppmv in (i–k) at 86, 80 and 75 km,

51 respectively. Dashed lines indicate planetary wave westward tilt with altitude.

52

53 **Time–longitude variations and vertical profiles of MLS temperature anomalies**



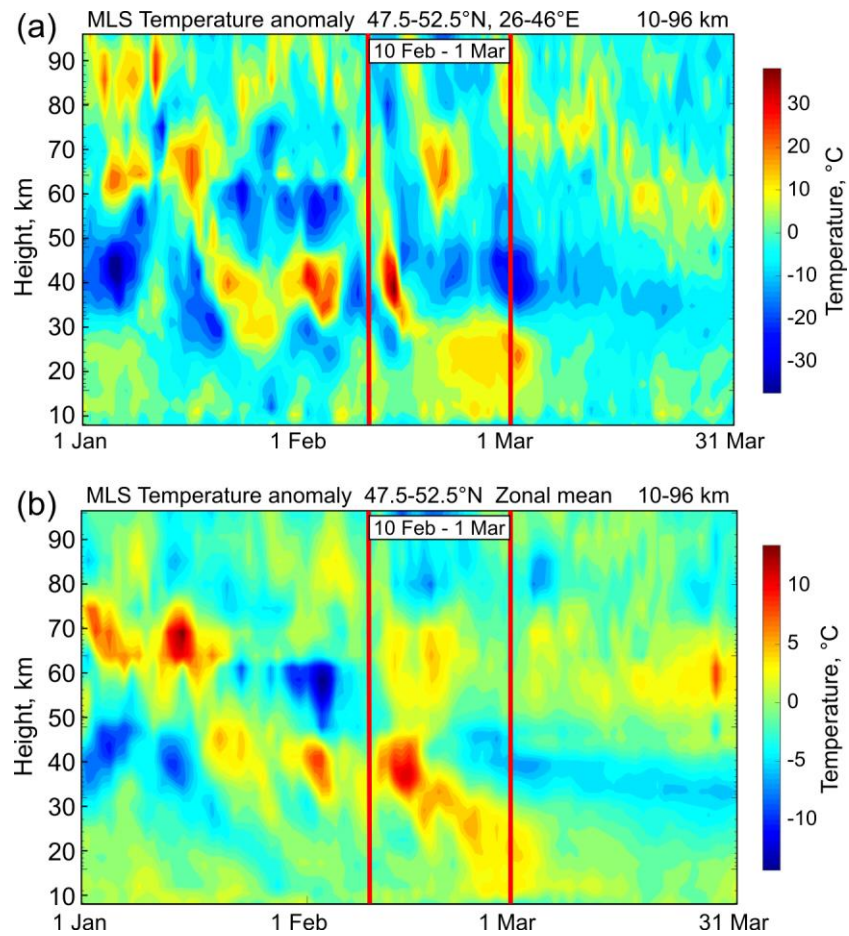
54

55

56 **Figure S3.** Time–longitude variations of the zonal anomalies in the MLS temperature in the  
 57 Kharkiv' zone 47.5–52.5°N with respect to the climatology 2005–2017 during January–March  
 58 2018. The ten MLS pressure levels between 46 hPa and 0.01 hPa (22 km to 81 km) are  
 59 presented. Solid (dashed) lines indicate the zonal wave 1 ridge (trough) slowly propagated  
 60 westward in time and simultaneously displaced westward with altitude. The latter tendency is  
 61 due to upward propagation of the planetary waves. Dotted lines in the plot for 42 km indicate  
 62 the change of the zonal anomaly propagation from eastward to westward near 10 February due  
 63 to zonal wind reverse from westerly to easterly at the start of the SSW 2018.

64





66

67 **Figure S4.** Vertical profiles of the MLS temperature anomalies in January–March 2018 with  
 68 respect to the mean climatology 2005–2017 over (a) region 47.5–52.5°N, 26–46°E centered at  
 69 Kharkiv and (b) 47.5–52.5°N zonal mean centered at the Kharkiv latitude. Red vertical lines  
 70 confine the SSW event 2018.

71

72